Available online at www.sciencedirect.com
SCIENCE DIRECT®
Coordination Chemistry Reviews 248 (2004) 881–901
COORDINATION CHEMISTRY REVIEWS
www.elsevier.com/locate/ccr

Review

Annual survey of organometallic metal cluster chemistry for the year 2002

Michael G. Richmond*

Department of Chemistry, University of North Texas, Denton, TX 76203, USA

Received 3 March 2004; accepted 3 March 2004

Contents

Abstract

The synthetic, mechanistic, and structural chemistry of organometallic metal cluster compounds is reviewed for the year 2002.

Keywords: Organometallic cluster compounds; Polynuclear compounds

1. Dissertations

The reaction between Cp^*NbCl_4 and ammonia produces the niobium nitrido complex $[Cp^*Nb(N)Cl]_3$. The intermediate $Cp^*Nb(NH_2)Cl_3(NH_3)$, which has been isolated and characterized, is suggested to serve as a precursor to the nitride cluster [1]. The ability of $[Fe_3(CO)_9E]^{2-}$ and $[HFe_3(CO)_9E]^-$ (where E = S, Se, Te) to participate in the construction of thin films attached to gold surfaces has been described. The solution-phase self-assembly of these chalcogenide-capped clusters on the gold substrate has been thoroughly investigated by traditional surface science methods. The homogeneous carbonylation of methanol to afford methyl formate using the catalyst precursors $[Et_4N]_2[Fe_3(CO)_9E]$ has been studied. Detailed kinetic studies reveal that the reaction exhibits a first-order dependence on the initially charged cluster and a quasi-second-order dependence on CO. The influence of methoxide ion on the reaction is discussed [2]. The reaction of $Os_3(CO)_{10}(MeCN)_2$ with 2,2-dimethyl-4-phenyl-1,3-dioxolane furnishes the η^2-vinyl bridged cluster $Os_3(CO)_{10}[\mu\text{-}CHCHC(H)OC(Me)_2OCH_2](\mu\text{-}H)$, whose identity was established by IR and NMR spectroscopies, and X-ray crystallography [3]. The synthesis and reactivity of the triangular phosphido-bridged cluster $Ir_3(\mu\text{-}PPh_2)_3(CO)_6$ has been reported. X-ray analysis reveals the presence of one short Ir–Ir bond and two long Ir–Ir bonds. VT NMR data confirm that the phosphido groups participate in a rapid flip-flop motion relative to the metal triangle. Added dmad reacts with this cluster to produce

* Fax: +1-940-565-3814.
E-mail address: cobalt@unt.edu (M.G. Richmond).

0010-8545/$ – see front matter © 2004 Elsevier B.V. All rights reserved.
doi:10.1016/j.ccr.2004.03.002

the cluster compound $Ir_3(\mu\text{-}PPh_2)_3(CO)_6(\mu\text{-dmad})$, which is shown to possess a diiridacyclobutene moiety by X-ray diffraction analysis. Parallel reactivity studies employing $Ir_2Rh(\mu\text{-}PPh_2)_3(CO)_5$ have been carried out, and the results are contrasted with the homometallic Ir_3 cluster [4]. The synthesis and structural characterization of the linear heterometallic compounds $[Me_2Pt(\mu\text{-}L)_2Ag_2(MeCN)_2]^{2+}$ and $[(OC)_3Fe(\mu\text{-}L)_2Ag_2(Et_2O)]^{2+}$ [where L = 2, 6-bis(diphenylphosphino)pyridine] have appeared. The luminescent properties of related acetylide-bridged Cu_4 clusters have also been examined and the results fully discussed [5]. The use of $Cp^*_2Rh_2(\mu\text{-}C_2S_4)$ as a building block for the construction of larger metal ensembles containing novel C_2S_4 ligand bonding modes is described. The Rh_4 cluster $[Cp^*_4Rh_4(C_2S_4)_2]^{2+}$ has been obtained from $Cp^*_2Rh_2(\mu\text{-}C_2S_4)$ under electrochemical conditions. Treatment of $Cp^*_2Rh_2(\mu\text{-}C_2S_4)$ with $[Cp^*Ru(MeCN)_3]^+$ and $[Cp^*Rh(MeCN)_3]^{2+}$ gives $[Cp^*_3Rh_2Ru(C_2S_4)]^+$ and $[Cp^*_6Rh_6(C_2S_4)_2]^{4+}$, respectively. The ability of the C_2S_4 ligand to function as an electron donor is discussed [6]. The mixed-metal clusters $PtRu_5C(CO)_{16}$ and $Pt_2Ru_4(CO)_{18}$ have been employed in the fabrication of carbon-supported Pt–Ru nanoparticles. The resulting nanoparticles have been characterized by XAS, STEM, and EDX measurements. The reductive condensation of $PtRu_5C(CO)_{16}$ and $Pt_2Ru_4(CO)_{18}$ into a bimetallic nanoparticle has been studied by using in situ EXAFS, temperature-programmed desorption, and STEM methodologies [7].

2. Homometallic clusters

2.1. Group 6 clusters

Thermolysis of $[CpM(CO)_3]_2$ (where M = Mo, W) in the presence of gray antimony in toluene at 180 °C gives $(\mu,\eta^5\text{:}\eta^5\text{-}C_{10}H_8)(\eta^5\text{-}C_5H_5)M_3(CO)_6(\mu_3\text{-Sb})$. Crystallographic analysis of each product confirms the coupling of the two Cp moieties that gives the observed fulvalene ligand [8]. The reaction of $Cp_2Cr_2(CO)_6$ with $R_2P(S)P(S)R_2$ (where R = Me, Et) gives the corresponding thiophosphinito complexes $CpCr(CO)_2(SPR_2)$. $CpCr(CO)_2(SPMe_2)$ undergoes desulfurization upon heating to produce $Cp_2Cr_2(CO)_4(\mu\text{-H})(\mu\text{-}PMe_2)_2$ and $Cp_3Cr_3(CO)_2(S)(PMe_2)$. The X-ray structure of the latter product (Fig. 1) consists of a Cr_3 triangle that is capped by a μ_3-S moiety. The Cr–Cr edges of this cluster are ligated by the two CO groups and the phosphido moiety [9].

Treatment of $CrCl_3(THF)_3$ with three equivalents of RLi (where R = Me_3CCH_2, Me_3SiCH_2) gives the following compounds R_4Cr and $[R_2Cr]_4$. The molecular structure of $(Me_3SiCH_2)_8Cr_4$ exhibits a regular cube structure containing μ_2-alkyl groups. The magnetic susceptibility data and the results of density functional theory calculations are discussed relative to the nature of the HOMO and LUMO levels in the latter cluster [10]. The

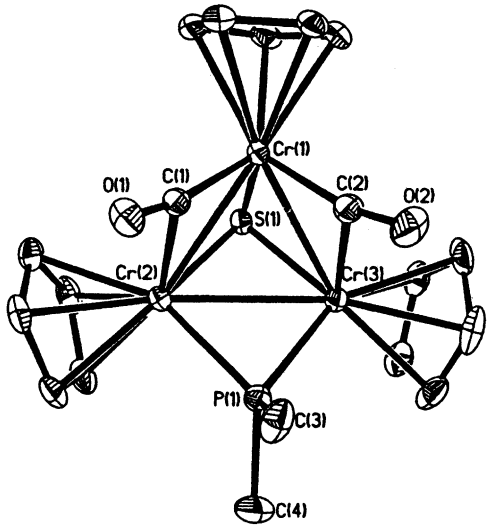

Fig. 1. X-ray structure of $Cp_3Cr_3(CO)_2(S)(PMe_2)$. Reprinted with permission from Organometallics. Copyright 2002 American Chemical Society.

synthesis of the novel hybrid metal-carbonyl-oxide cluster $[(OC)_5WSbW_3(CO)_9(\mu_3\text{-OMe})_2(\mu_3\text{-O})WO_2(OMe)]^{2-}$ from $W(CO)_6$ and $NaSbO_3$ is described. The molecular structure has been established by X-ray crystallography [11]. Thermolysis of $CpCr(CO)_2(\eta^2\text{-}S_2CNR_2)$ (where R = Me, Et, ^{i}Pr) gives $CpCr(CO)_2(\eta^2\text{-}SCNR_2)$, $Cp_6Cr_8(\eta^2\text{:}\eta^4\text{-}SCNR_2)_2$, $Cp_6Cr_8(\eta^1\text{:}\eta^2\text{-}S_2CNR_2)_2$, and $Cp_4Cr_4S_4$, in addition to minor amounts of other products. The X-ray structures of selected $Cp_6Cr_8S_8$ derivatives are presented and the structural highlights are discussed [12].

2.2. Group 7 clusters

The reaction of the disulfide complex $Mn_2(CO)_7(\mu\text{-}S_2)$ with SMe_2 affords the new complexes $Mn_2(CO)_6(\mu\text{-}S_2)(\mu\text{-}SMe_2)$ and $Mn_4(CO)_{14}(SMe_2)(\mu_3\text{-}S_2)(\mu_4\text{-}S_2)$. The same starting material has been explored for its reactivity with thietane and 1,4,9-trithiacyclododecane, with similar reaction products being found as in the SMe_2 reactions. The solution spectroscopic data are described, and the structural highlights of four compounds are discussed [13]. Treatment of $Mn_2(CO)_9(MeCN)$ with thiirane yields $Mn_2(CO)_7(\mu\text{-}S_2)$, $Mn_4(CO)_{15}(\mu_3\text{-}S_2)(\mu_4\text{-}S_2)$, and $Mn_4(CO)_{14}(MeCN)(\mu_3\text{-}S_2)(\mu_4\text{-}S_2)$, via sulfur transfer from the thiirane substrate. The dimanganese disulfide complex $Mn_2(CO)_7(\mu\text{-}S_2)$ reacts with tertiary phosphines and arsines to furnish a variety of Mn_4 and Mn_6 derivatives. The structural features of the accompanying eight X-ray structures are thoroughly discussed [14]. The synthesis, spectral properties, and X-ray diffraction structure of the tetramanganese complex $(\mu_3\text{-}CS_3)_2Mn_4(CO)_{16}$, which has been prepared from $Mn_2(CO)_{10}$ and CS_2, have been published. This same product is also obtained from the reaction of selected $(\eta^2$-dithiocarboxylato)$Mn(CO)_4$ complexes with CS_2 [15].

2.3. Group 8 clusters

The mechanism associated with the very low energy fluxional process in $Fe_3(CO)_{12}$ has been reexamined. A process involving the movement of the ligand icosahedron about the central Fe_3 triangle is discussed and rejected. The failed criteria for previously proposed fluxional processes are discussed [16]. The use of surface organometallic chemistry in the preparation of alkyne-substituted clusters has been described. Treatment of $Ru_3(CO)_{12}$ that has been deposited on a wide variety of substrates with *tert*-butyl acetylene, 2-methyl-1-butyn-3-ol, or 3-phenyl-1-butyn-3-ol gives the corresponding triruthenium acetylide- and acetylene-substituted clusters under mild conditions. The factors that affect the reaction rates and yields are discussed, and data from electron microscopy studies are used in the formulation of a working reaction mechanism [17]. Picosecond time-resolved IR spectral data have allowed for the first direct observation of a CO-bridged intermediate from $Ru_3(CO)_{12}$ during near-UV photolysis. The formation of a CO-bridged $Ru_3(CO)_{12}$ isomer as the primary photoproduct is in agreement with the structure of the reactive isomer of $Ru_3(CO)_{12}$ that has been postulated earlier in the literature [18]. A report on the efficient and novel chelation-assisted hydroesterification of alkenes using $Ru_3(CO)_{12}$ has appeared. The details associated with this reaction, which relies on the presence of a 2-pyridyl moiety to assist in the chelation of the ruthenium catalyst, and a crude working mechanism are presented [19]. The $Ru_3(CO)_{12}$-catalyzed synthesis of pyranopyrandiones via the reconstructive carbonylation of cyclopropenones has been described. A mechanism based on the results of a ^{13}CO labeling study is discussed [20]. $Ru_3(CO)_{12}$, in the presence of dimethyl(2-pyridyl)(vinyl)silane, is reported to function as a catalyst for the intermolecular Pauson–Khand reaction. The efficiency of the reaction, regioselectivity, and the effect of the removable 2-$PyMe_2Si$ moiety on the course of the reaction are discussed [21]. A report on the synthesis of cyclic imides and anhydrides using $Fe_3(CO)_{12}$, amines, and alkynes has appeared [22].

The reactivity of 1-pentyne and acetylene with $H_2Os_3(CO)_{10}$ in the presence of *para*-H_2 has been investigated. Data from mechanistic studies are discussed relative to catalytic intermediates pertinent to catalytic hydrogenation. Of the four different triosmium clusters that were spectroscopically observed in solution, only the σ-π-vinyl complex $Os_3(CO)_{10}(\mu,\eta^2\text{-CH=CHR})(\mu\text{-H})$ undergoes reaction with added H_2 to afford the corresponding alkene cluster product [23]. Photolysis of $Fe_3(CO)_9(\mu_3\text{-CF})_2$ with 1,1-difluoroallene yields the cluster compounds octacarbonyl(μ_3-fluoromethylidyne)($\mu,\eta^1{:}\eta^3{:}\eta^1$-1,3-difluoro-2-fluoromethylpropane-1,2,3-triyl)triiron and nonacarbonyl($\mu,\eta^1{:}\eta^2{:}\eta^1$-1-fluoro-2-trifluoromethylbut-1-en-1-yl-4-ylidyne)triiron. The solution ^1H NMR data and the molecular structures, as established by X-ray diffraction analyses, are discussed [24]. A report on the hydrogenation of benzene using the water-soluble cluster $[(\eta^6\text{-}C_6H_6)(\eta^6\text{-}C_6Me_6)_2Ru_3(\mu_3\text{-O})(\mu\text{-H})_3]^+$ has appeared. Rapid reaction rates and high turnover numbers are reported. Similar benzene hydrogenation activity is also observed when the hydroxy-bridged cluster $[(\eta^6\text{-}C_6H_6)(\eta^6\text{-}C_6Me_6)_2Ru_3(\mu_3\text{-O})(\mu\text{-H})_2(\mu\text{-OH})]^+$ is employed as the catalyst precursor. The hydrogenation activity was found to be unchanged when these reactions were carried out in the presence of added mercury, suggesting that intact Ru_3 clusters serve as the active catalysts [25]. The reactivity of $[Ru_3(\mu\text{-Cl})(CO)_{10}]^-$ with various substituted butyne derivatives has been examined. The resulting butyne-substituted ruthenium clusters were explored for their proparagylic activation, which affords the allenyl cluster $Ru_3(\mu\text{-Cl})(CO)_9(\mu,\eta^3\text{-}CH_3CCCH_2)$. The nucleophilic reactivity of this latter cluster has been studied with the aid of MO calculations [26]. The triosmium cluster $HOs_3(CO)_{10}(\eta^1{:}\eta^1\text{-}OC_4H_2CCH_3)$ has been allowed to react with a series of aromatic aldehydes to yield coupling products via an aldol reaction sequence. The X-ray structure of the product from the benzaldehyde reaction confirms the condensation reaction [27]. A triple-decker triruthenium metallabenzene cluster has been synthesized from $[Cp^*Ru(H_2O)(nbd)]^+$ in the presence of HCO_2Na, followed by treatment with HBF_4. The initially formed complex is the diruthenium species $Cp^*_2Ru_2(C_7H_8)$, which slowly decomposes to furnish $[Cp^*RuEtCpRuCp^*]^+$, $Cp^*RuEtCp$, and the triple-decker complex $[Cp^*_3Ru_3(C_7H_8)(\mu\text{-H})]^{2+}$, whose X-ray structure accompanies this report [28]. The activation of acetylene by $Cp^*_3Ru_3(\mu\text{-H})_3(\mu_3\text{-H})_2$ has been explored, with the μ_3-ethylidene-$\eta^2(\|)$-ethyne complex $Cp^*_3Ru_3(\mu\text{-H})_3(\mu\text{-CMeH})[\mu_3\text{-}\eta^2(\|)\text{-CH=CH}]$ being formed from $Cp^*_3Ru_3(\mu\text{-H})_3(\mu\text{-}\eta^1{:}\eta^2\text{-CH=CH}_2)_2$. The α-C–H bond of the μ-ethylidene ligand in the former cluster undergoes oxidative addition and loss of hydrogen upon heating to produce $Cp^*_3Ru_3(\mu\text{-H})_2(\mu_3\text{-CMe})[\mu_3\text{-}\eta^2(\|)\text{-CH=CH}]$. VT NMR data on this latter cluster reveal that both the μ_3-ethyne and hydride ligands are fluxional at ambient temperatures. $Cp^*_3Ru_3(\mu\text{-H})_2(\mu_3\text{-CMe})[\mu_3\text{-}\eta^2(\|)\text{-CH=CH}]$ reacts with added acetylene to give $Cp^*_3Ru_3[\mu_3\text{-}\eta^1{:}\eta^3{:}\eta^1\text{-C(H)-C(H)CMe}](\mu_3\text{-CMe})(\mu\text{-H})$. The molecular structure (Fig. 2) confirms the existence of the μ_3-η^3-diruthenaallyl moiety in this last product. Ligand exchange schemes and plausible reaction mechanisms that account for the formation of the observed products are presented and discussed [29].

Thermolysis of 2-methyl-1-buten-3-yne in the presence of $Fe_3(CO)_{12}$ yields four main products, of which the open-cluster isomers of $Fe_3(CO)_{10}[H_2CC(Me)CC(H)\text{-}C(H)C(CO)C(Me)CH_2]$ and $Fe_3(CO)_{10}[HCC(Me)C(H)\text{-}C(H)C(H)C(CO)C(Me)CH_2]$ have been isolated and structurally characterized. The tail-to-tail dimerization of the alkyne ligand and reaction pathways are discussed [30]. The reaction of $Ru_3(\mu\text{-H})(\mu_3\text{-CCCPh}_2)(\mu\text{-OH})(CO)_9$ with alkynes and 1,3-diynes has been investigated. Use of HC_2SiMe_3 led to the sequential formation of $Ru_3[\mu_3\text{-CH(SiMe}_3)CHCC{=}CPh_2](\mu\text{-OH})(CO)_9$ and

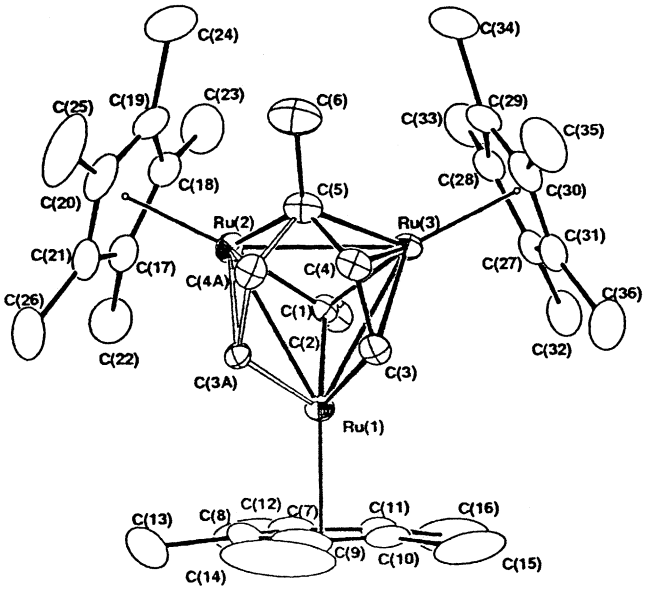

Fig. 2. X-ray structure of $Cp^*_3Ru_3[\mu_3\text{-}\eta^1\text{:}\eta^3\text{:}\eta^1\text{-}C(H)C(H)CMe](\mu_3\text{-}CMe)(\mu\text{-}H)$. Reprinted with permission from Organometallics. Copyright 2002 American Chemical Society.

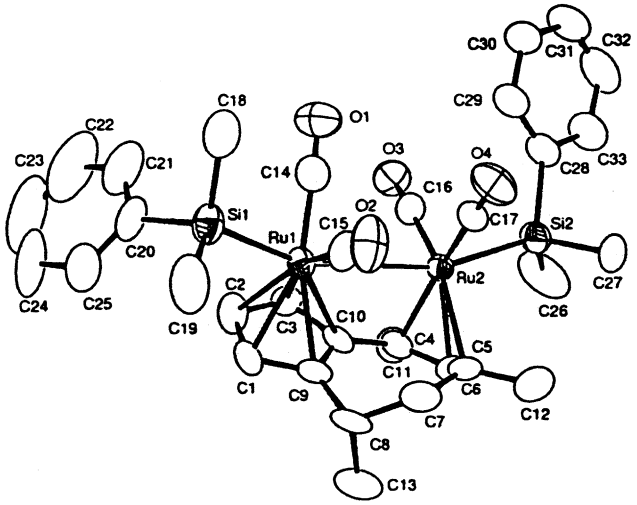

Fig. 3. X-ray structure of $Ru_3(H)(SiMe_2Ph)(CO)_6(\mu_2\text{-}\eta^3\text{:}\eta^5\text{-}4,5\text{-dihydro-}4,6,8\text{-trimethylazulene})$. Reprinted with permission from Organometallics. Copyright 2002 American Chemical Society.

$Ru_3(\mu_3\text{-}CRCR'CR'CRCC{=}CPh_2)(CO)_8$. Other acetylenic substrates explored include FcCCH, PhCCPh, and FcCC-CCFc. The characterization of the new clusters by ^1H and IR spectroscopies is described, and the molecular structures of eight products are presented and discussed [31]. The results from detailed NMR studies (^1H, ^{13}C, ^{29}Si) on acetylide-substituted and the parallel alkyne ligand in Ru_3 and Os_3 clusters have been published. The NMR data are contrasted with the results of extended Hückel MO calculations. The X-ray structures of $(\mu\text{-}H)Ru_3(CO)_9(CCR)$ (where R = $SiMe_3$, $SiPh_3$) and $(\mu\text{-}H)Os_3(CO)_9(CCR)$ (where R = $SiPh_3$, Bu^t) have been determined and the structural highlights described [32]. Oxidative addition of $PhMe_2SiH$ to $Ru_3(CO)_7(\mu_3\text{-}\eta^5\text{:}\eta^5\text{-}4,6,8\text{-trimethylazulene})$ takes place by CO loss and hydrogenation of one of the azulene carbon-carbon double bonds to furnish the 46-election cluster $Ru_3(H)(SiMe_2Ph)(CO)_6(\mu_2\text{-}\eta^3\text{:}\eta^5\text{-}4,5\text{-dihydro-}4,6,8\text{-trimethylazulene})$, whose X-ray structure is shown in Fig. 3. Both the starting cluster and the product exhibit moderate catalytic activity in the hydrosilation of acetophenone. The NMR data that support a catalytic cycle based on an intact triruthenium cluster are thoroughly discussed [33].

The reactivity of the triruthenium clusters $Ru_3(CO)_{10}(MeCN)_2$ and $Ru_3(CO)_{10}$(dppm) with the ferrocenylalkynes FcC_2H, HC_2C_2Fc, and FcC_2C_2Fc has been investigated and found to afford $Ru_3(CO)_9(\mu\text{-}CO)(\mu_3\text{-}RC_2R')$, $Ru_3(CO)_7(\mu\text{-}H)(\mu_3\text{-}C_2CCFc)(\mu\text{-dppm})$, $Ru_3(CO)_7(\mu\text{-}CO)(\mu_3\text{-}FcC_2CCFc)(\mu\text{-dppm})$, and $Ru_3(CO)_5(\mu\text{-}CO)[\mu_3\text{-}C_4Fc_2(CCFc)_2](\mu\text{-dppm})$. The solution spectral data are presented, and the molecular structures of four X-ray structures are discussed relative to other structurally characterized ferrocenylalkyne complexes. The redox behavior of several of these clusters has been studied by cyclic voltammetry [34]. $Os_3(CO)_{11}(MeCN)$ has been allowed to react with 1,4-bis(ferrocenyl)butadiyne to furnish the cluster compounds $Os_3(CO)_{10}(\mu_3\text{-}\eta^2\text{-}FcC_4Fc)$ and $Os_3(CO)_{11}(\mu_3\text{-}\eta^4\text{-}FcC_4Fc)$. The latter cluster has been obtained in essentially quantitative yield when $Os_3(CO)_{10}(MeCN)_2$ is employed as the starting material. The molecular structure of the decacarbonyl product displays a triangular osmium core that contains a triply bridged alkyne moiety. The X-ray structure of $Os_3(CO)_{11}(\mu_3\text{-}\eta^4\text{-}FcC_4Fc)$ exhibits an open triosmium core where the two alkyne groups are coordinated in a parallel fashion to the three osmium centers. Treatment of $Os_3(CO)_{10}(MeCN)_2$ with 1,4-bis(ferrocenyl)butadiyne at elevated temperatures gives the dinuclear complex $Os_2(CO)_6(\mu\text{-}\eta^4\text{-}FcC_2CCFc)$. Thermolysis of $Os_3(CO)_{10}(\mu_3\text{-}\eta^2\text{-}FcC_4Fc)$ leads to alkyne cleavage and the new cluster $Os_3(CO)_9(\mu_3\text{-}\eta^2\text{-}C_4Fc)(\mu\text{-}\eta^2\text{-}CCFc)$, whose molecular structure was established by X-ray diffraction analysis. The electrocommunication between the ferrocene centers in these products was explored by cyclic and differential pulse voltammetric techniques. The MO properties of $Os_3(CO)_{11}(\mu_3\text{-}\eta^4\text{-}FcC_4Fc)$ were studied by extended Hückel calculations using the model bis(dehydrobutatriene) complex $Os_3(CO)_{11}(C_4H_2)$ [35]. The coordination of 1,12-bis(ferrocenyl)-1,3,5,7,9,11-dodecahexayne, which was synthesized from the oxidative coupling of $FcC_2C_2C_2H$, to $Os_3(CO)_{11}(MeCN)$ has been achieved. The product of this reaction, $Os_6(CO)_{22}(\mu_6\text{-}\eta^8\text{-}FcC_4CCCCC_4Fc)$, contains two open Os_3 clusters that are coordinated parallel to opposite sides of the hexayne chain. The same ligand reacts with $Co_2(CO)_8$ to give $Co_8(CO)_{24}$ $(\mu_8\text{-}\eta^2\text{:}\eta^2\text{:}\eta^2\text{:}s\eta^2\text{-}FcC_2CCC_4CCC_2Fc)$. The X-ray structures of the Os_6 and Co_8 complexes are presented and the structural features are discussed. Differential pulse voltammetric data on the starting ligand and the two clusters

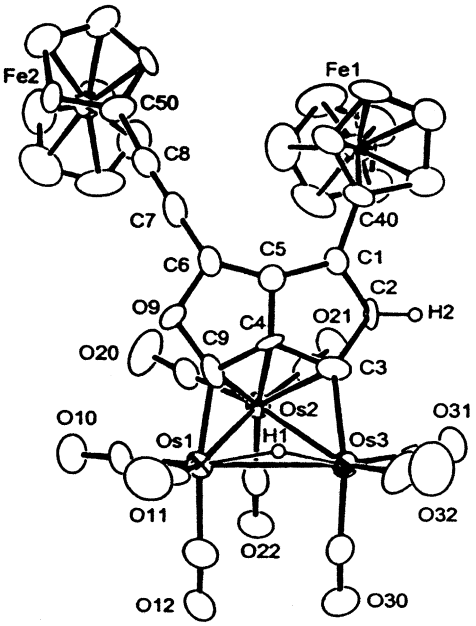

Fig. 4. X-ray structure of $Os_3(CO)_9(\mu_3\text{-}\eta^3\text{-}FcCCHC_4COCCFc)(\mu\text{-}H)$. Reprinted with permission from Organometallics. Copyright 2002 American Chemical Society.

indicate that there is no detectable electronic communication between the two ferrocenyl centers [36]. The new clusters $Os_3(CO)_9(\mu_3\text{-}\eta^3\text{-}FcCCHC_4COCCFc)(\mu\text{-}H)$, $Os_3(CO)_{10}(\mu_3\text{-}\eta^2\text{-E-}FcCHCHC_2CCCCFc)$, and $Os_6(CO)_{20}(\mu_3\text{:}\mu_3\text{-}\eta^2\text{:}\eta^2\text{-E,E-}FcCHCHC_2\text{-}C_2CHCHFc)$ have been obtained from the reaction of $Os_3(CO)_{10}(\mu\text{-}H)_2$ with 1,8-bis(ferrocenyl)octatetrayne. The three products were characterized in solution by IR and ^1H NMR spectroscopies, in addition to X-ray crystallography. The molecular structure of $Os_3(CO)_9(\mu_3\text{-}\eta^3\text{-}FcCCH_2C_4COCCFc)(\mu\text{-}H)$ (Fig. 4) reveals the presence of a tetrayne chain that is coupled to a CO ligand and that has been cyclized to form an eight-membered heterobicyclic ring. CV and DPV data indicate that the two ferrocenyl moieties in the Os_3 cluster undergo two separate one-electron oxidations consistent with inequivalent ferrocenyl groups. A working reaction mechanism involving hydride transfer to a coordinated alkyne group is presented and discussed [37].

A detailed structural and spectroscopic study of the dihydrogen bond in the imine-substituted cluster $H(\mu\text{-}H)Os_3(CO)_{10}(HN{=}CPh_2)$ has been published. ^1H NMR measurements have given an interproton distance for the ancillary hydrides that is ca. 0.11 Å longer then the value determined by X-ray analysis. This difference between the NMR and diffraction data distances is explained in terms of an amplitude oscillatory motion of the imine relative to the N–Os coordination site and intramolecular hydrogen bonding between imine N–H group and the Os–H moiety [38]. Treatment of $Os_3(CO)_8(CNR)(\mu_3\text{-}CNR)(\mu_3\text{-}\eta^1\text{:}\eta^2\text{:}\eta^1\text{-}C_{60})$ (where R = benzyl) with Me_3NO, followed by thermolysis reactions with different $2e^-$ donor ligands, gives the corresponding substitution products $Os_3(CO)_7(CNR)(\mu_3\text{-}CNR)L(C_{60})$. The C_{60} coordination mode to the osmium frame remains unchanged for the ligands $(\mu\text{-}H)_2$, CNR, and PMe_3. When PPh_3 is employed as the incoming ligand, an orbital reorganization of the C_6 ring of C_{60} is observed, leading to a $\mu_3\text{-}\eta^1\text{:}\eta^1\text{:}\eta^2\text{-}C_{60}$ ligand. Full solution characterization by ^1H, ^{13}C, and 2D ^1H–^1H COSY NMR spectroscopic methods are presented, and the molecular structures of all four new products are included with this report [39]. A report on the versatility of [60] fullerene as a $4e^-$ donor ligand to triosmium clusters has appeared. Substitution of CO by PPh_3 in $Os_3(CO)_8(CNR)(\mu_3\text{-}CNR)(\mu_3\text{-}\eta^1\text{:}\eta^2\text{:}\eta^1\text{-}C_{60})$ (where R = benzyl) leads to a 1,2-σ-type C_{60} ligand in the product cluster $Os_3(CO)_7(PPh_3)(CNR)(\mu_3\text{-}CNR)(\mu_3\text{-}\eta^1\text{:}\eta^1\text{:}\eta^2\text{-}C_{60})$. While these two Os_3 clusters are reversibly interconverted, treatment of the latter cluster with additional PPh_3 gives the π-type C_{60} cluster $Os_3(CO)_6(PPh_3)(CNR)(\mu_3\text{-}CNR)(\mu\text{-}PPh_2)(\mu_3\text{-}\eta^2\text{:}\eta^2\text{-}C_{60})$. The X-ray structure of this phosphido-bridged cluster reveals that one of the three osmium–osmium bonds has been cleaved during the reaction [40]. High-temperature thermolysis of $Os_3(CO)_9(\mu_3\text{-}\eta^2\text{:}\eta^2\text{:}\eta^2\text{-}C_{60})$ with added $PhCH_2N{=}PPh_3$ produces the benzyl isocyanide-substituted cluster $Os_3(CO)_8(CNR)(\mu_3\text{-}\eta^2\text{:}\eta^2\text{:}\eta^2\text{-}C_{60})$ in good yield. Photolysis of the same $Os_3(CO)_9$ cluster with CNR (where R = benzyl) gives the μ_3-capped cluster $Os_3(CO)_9(\mu_3\text{-}CNR)(\mu_3\text{-}\eta^1\text{:}\eta^2\text{:}\eta^1\text{-}C_{60})$. NMR and X-ray data on these clusters are presented and discussed relative to the structural interconversions exhibited the C_{60} ligand [41]. Ligand substitution in $Fe_2Ru(CO)_{12}$ and $FeRu_2(CO)_{12}$ by $CNBu^t$ and CNCy has been studied. The molecular structures of four clusters have been solved and discussed relative to the parent carbonyl cluster [42].

The reaction of $Ru_3(CO)_{12}$ with excess 3,5-di-*tert*-butylpyrazole at 170 °C gives the unsaturated pyrazolate-bridged dimer $Ru_2(CO)_5(dbpz)_2$ [43]. The reactivity of *para*-hydrogen with a series of μ_3-quinolyl triosmium clusters has been investigated. The mechanistic information that was obtained is discussed with respect to the hydrogenation of coordinated heterocyclic moieties at triosmium clusters [44]. The acid–base chemistry of electron-deficient benzoheterocycle triosmium clusters has been examined. The clusters have the general structure $Os_3(CO)_9(\mu_3\text{-}\eta^2\text{-L-}H)(\mu\text{-}H)$ (where L = various heterocycles). Detailed NMR assignments are presented, and the molecular structure of $Os_3(CO)_9(\mu_3\text{-}\eta^2\text{-phenanthridine})(\mu\text{-}H)$ is included in this report [45]. The coordination chemistry of 2-amino-7,8-benzoquinoline at triruthenium and triosmium clusters has been explored. The heterocycle reacts with $Ru_3(CO)_{10}(MeCN)_2$ to initially give $Ru_3(\mu_3\text{-}\eta^3\text{-abq-}C,N,N)(CO)_9$. This product reacts with additional ligand to give $Ru_3(\mu\text{-}H)_2(\mu_3\text{-}\eta^3\text{-abq-}C,N,N)_2(CO)_6$. The cyclometalated abq ligands bond to a Ru–Ru edge via the nitrogen atom of an amido fragment and chelate to the remaining ruthenium center by the quinoline N atom and the C atom of the cyclometalated rings, as established by X-ray crystallog-

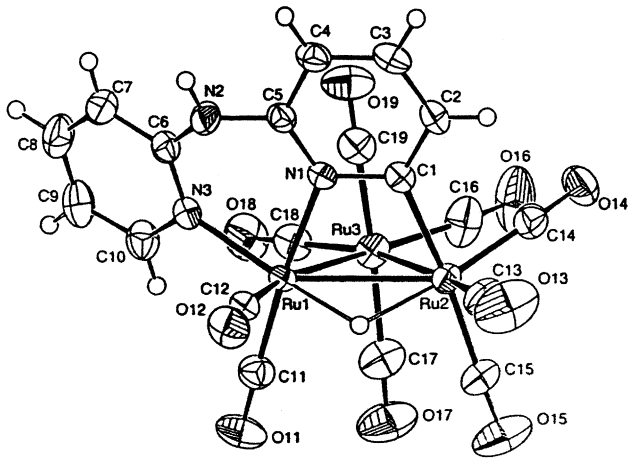

Fig. 5. X-ray structure of $Ru_3(\mu\text{-H})(CO)_9(\mu\text{-}\eta^3\text{-dpa-C,N,N})$. Reprinted with permission from Organometallics. Copyright 2002 American Chemical Society.

raphy. $Os_3(CO)_{10}(MeCN)_2$ reacts with the same heterocycle to produce $Os_3(\mu\text{-H})(CO)_{10}(\mu\text{-}\eta^1\text{-Habq-N})$, which is shown to be stable towards further reaction in refluxing toluene. The Os_3 cluster was characterized in solution by IR and NMR spectroscopies [46]. The first examples of trimetal clusters containing ligands derived from di(2-pyridyl)amine have been synthesized from $Ru_3(CO)_{12}$ and $M_3(CO)_{10}(MeCN)_2$ (where M = Ru, Os). The cluster $Ru_3(\mu\text{-H})(CO)_9(\mu\text{-}\eta^3\text{-dpa-C,N,N})$ chelates a ruthenium center via both pyridine nitrogens and is attached to an adjacent ruthenium atom through the C atom of a metalated pyridine ring (Fig. 5). The triosmium cluster $Os_3(CO)_{10}(MeCN)_2$ shows different reactivity with the dpa ligand, with $Os_3(\mu\text{-H})(CO)_{10}(\mu\text{-}\eta^2\text{-dpa-N,N})$ and $Os_3(\mu\text{-H})(CO)_9(\mu_3\text{-}\eta^2\text{-dpa-N,N})$ being formed in a stepwise sequence. The dpa ligand is attached in an edge-bridging and face-capping fashion, respectively, in these Os_3 clusters [47].

Alkene bond migration in N-allylic substrates has been catalyzed by the chiral clusters $(\mu\text{-H})Os_3(CO)_{10}(\mu\text{-OCNRR}')$. The utility of these chiral clusters as stereodifferentiating catalysts for asymmetric isomerizations is discussed [48]. The reaction of the unsaturated cluster $Os_3(\mu\text{-H})_2(CO)_{10}$ with various amine ligands has been investigated. The expected complexes $Os_3H(\mu\text{-H})(CO)_{10}(\text{amine})$ were evaluated by ^{1}H NMR spin-lattice relaxation spectroscopy, and the observation of an unconventional M–H···H–N hydrogen-bond in these clusters has been verified. The effect of the pK_b on the unconventional H···H bond has been quantified through the use of T_1 values from selectively deuterated isotopomers. DFT calculations have been carried out on complexes $Os_3H(\mu\text{-H})(CO)_{10}(NH_2CH_2Ph)$, and the various coordination geometries of the amine on the surface of the Os_3 cluster are described. No ligand basicity trends were found when the amine-substituted clusters were studied by ^{187}Os NMR spectroscopy [49]. $Os_3(CO)_{11}(MeCN)$ has been allowed to react with (*R*)-(+)-1-phenylethylamine to give the diastereomeric clusters $(\mu\text{-H})Os_3(CO)_{10}[\mu\text{-OCNH-(}R\text{)-CHMePh}]$ in a 1:2 ratio. The ^{1}H NMR and IR spectroscopic data and the $[\alpha]_D$ values are reported for each diastereomer. The absolute configuration of the (+)-diastereomer was ascertained by X-ray diffraction analysis [50]. The light-induced formation of zwitterions and biradicals from the cluster $Os_3(CO)_{10}(^i\text{Pr-Acpy})$ is reported. The effect of the solvent on the excited state(s) of the cluster has been assessed through the use of picosecond UV-Vis and nanosecond IR spectroscopy [51]. $Os_3(CO)_{10}(\alpha\text{-diimine})$ has been examined by ultrafast time-resolved absorption spectroscopy and the primary photoprocesses have been established. Both biradicals and zwitterionic species are observed upon decay of the excited cluster, depending upon the nature of the reaction solvent. These data reveal that a coordinating solvent such as MeCN may induce both homolytic and heterolytic cleavage of an Os–Os bond in this genre of cluster [52].

The reaction of the diphosphene ligand (*E*)-bis(2,4,6-tri-*tert*-butylphenyl)diphosphene with $M_3(CO)_{12}$ (where M = Fe, Ru) has been studied. Cluster fragmentation of $Fe_3(CO)_{12}$ occurs, with $Fe(CO)_4(\eta^1\text{-diphosphene})$ being formed as the major product. Thermolysis of the diphosphene with $Ru_3(CO)_{12}$ affords the bis(phosphido)-bridged cluster $Ru_3(\mu\text{-H})_2(CO)_8(\mu\text{-}PC_6H_2\text{-2,4-}^t\text{Bu-6-}CMe_2CH_2)_2$, whose X-ray structure confirms the C–H bond activation of one of the three *t*-butyl groups. Preliminary studies indicate that the cluster product is able to hydrogenate alkenes and alkynes without fragmentation of the Ru_3 core [53]. The clusters $Ru_3[\mu\text{-}cyclo\text{-}(PhX)_6](CO)_{10}$ (where X = P, As) have been isolated from the reaction of $Ru_3(CO)_{10}(MeCN)_2$ with *cyclo*-$(PhX)_6$ at ambient temperatures. The ancillary ligand in each cluster contains an intact six-membered ring that adopts a chair conformation and that bridges a Ru–Ru edge through two phosphorus or arsine atoms in the 1,5-positions of the ring. Thermolysis of $Ru_3(CO)_{12}$ with the same ligands leads to ligand fragmentation and formation of $Ru_4(CO)_{13}(\mu_3\text{-AsPh})_2$ and $Ru_6(CO)_{12}(\mu_4\text{-PPh})_3(\mu_3\text{-PPh})_2$. Similar reactivity is observed in the thermolysis of *cyclo*-$(PhAs)_6$ with $Fe_3(CO)_{12}$. Here, $Fe_3(CO)_9(\mu_3\text{-AsPh})_2$ was isolated as the sole product. The analogous cluster $Fe_3(CO)_9(\mu_3\text{-PPh})_2$ and the dinuclear species $Fe_2(CO)_6[\mu\text{-}\eta^2\text{-}catena\text{-}(P_4Ph_4)]$ and $[Fe_2(CO)_6\{\mu_4\text{-}(P_2Ph_2)\}]_2$ were isolated from the reaction of $Fe_3(CO)_{12}$ with *cyclo*-$(PhP)_6$ at elevated temperature. Detailed solution IR and NMR data are reported, and the molecular structures of four cluster products are presented, with their unique structural features discussed [54]. The hydrogenation and isomerization of 1-hexene using the catalyst precursors $Ru_3(CO)_9(PPh_3)_3$ and $Ru_3(CO)_9[Ph_2PCH_2CH_2Si(OMe)_3]$ have been explored. Both catalysts were heterogenized in silica matrices by sol–gel methodology and their catalytic activity assessed by UV-Vis and FT-IR spectroscopies. Higher catalytic activity in the hydrogenation of 1-hexene was found with the gel immobilized catalysts as compared to the homogeneous Ru_3 systems. The formation of catalytically active

$[Ru(II)(CO)_2]_n$ species within the porous matrix is postulated to be responsible for the observed reactivity trends [55]. Phosphine substitution in $Ru_3(CO)_{10}(\mu$-dppm) at room temperature gives $Ru_3(CO)_9(PR_3)(\mu$-dppm) (where R = Et, Ph, Cy, ^{i}Pr). X-ray structural data suggest that variations in the Ru–Ru bond adjacent to the phosphine ligand are responsible for the enhanced reactivity of $Ru_3(CO)_{10}(\mu$-dppm) relative to the parent cluster $Ru_3(CO)_{12}$. The data are consistent with the inability of $Ru_3(CO)_{10}(\mu$-dppm) to relieve steric congestion within the cluster, as imposed by the bulky dppm ligand [56]. High-temperature thermolysis of $Os_3(CO)_{10}(\mu$-dppm) with H_2S furnishes the known cluster $(\mu\text{-}H)_2Os_3(CO)_7(\mu_3\text{-}S)(\mu$-dppm) and the new cluster $Os_3(CO)_7(\mu_3\text{-}CO)(\mu_3\text{-}S)(\mu$-dppm). Use of thiourea in place of H_2S gives the former product in high yield. The stereoisomeric $50e^-$ clusters $Os_3(CO)_7(\mu_3\text{-}S)_2(\mu$-dppm) have been isolated from the reaction of $Os_3(CO)_{10}(\mu$-dppm) with tetramethylthiourea. Independent reactions of $Os_3(CO)_7(\mu_3\text{-}CO)(\mu_3\text{-}S)(\mu$-dppm) with added tetramethylthiourea confirm the formation of the two stereoisomeric $50e^-$ clusters. Treatment of this same heptacarbonyl Os_3 cluster with H_2 yields the aforementioned dihydride cluster. The details associated with the three X-ray structures that are present are discussed [57]. The cyclization of allenylidene ligands to indenyl groups has been demonstrated in thermolysis reactions of $Ru_3(CO)_7(\mu\text{-}CO)(\mu\text{-dppm})(\mu_3\text{-}C{=}C{=}CR_2)$ (where R = Ph, tol). The X-ray structure of $Ru_3(CO)_5(\mu_3\text{-}PPhCH_2PPh_2)(\mu_3\text{-}C_9H_5Ph_2)$ is reported and the course of indenyl ring formation is discussed. Treatment of $Ru_3(\mu\text{-}H)(CO)_9(\mu\text{-}OH)(\mu_3\text{-}C{=}C{=}CPh_2)$ with $Co_2(CO)_8$ in refluxing toluene gives $CoRu_3(CO)_5(\mu\text{-}CO)_4(\mu_3\text{-}C_9H_6Ph)$, whose molecular structure consists of a tetrahedral $CoRu_3$ core, where the three Co–Ru edges are bridged by CO ligands. The Ru_3 face is capped by a 1-phenylindenyl ligand that is attached to two ruthenium centers by η^2 interactions and by an η^5 interaction to the remaining ruthenium center [58]. Thermolysis of $Ru_3(CO)_{10}(Ph_2PC_2Bu^t)_2$ gives the $48e^-$ phosphido-bridged cluster $Ru_3(CO)_6(\mu\text{-}PPh_2)_2(\mu\text{-}\eta^1{:}\eta^2\text{-}C_2Bu^t)_2$. Ligand addition to this cluster readily furnishes the corresponding $50e^-$ clusters $Ru_3(CO)_6L(\mu\text{-}PPh_2)_2(\mu\text{-}\eta^1{:}\eta^2\text{-}C_2Bu^t)_2$. Thermolysis of the related clusters $Ru_3(CO)_{10}(Ph_2PC_2Ph)(Ph_2PC_2R)$ (where R = Ph, Bu^t) produces the $50e^-$ clusters $Ru_3(CO)_7(\mu\text{-}PPh_2)_2(\mu\text{-}\eta^1{:}\eta^2\text{-}C_2Ph)(\mu\text{-}\eta^1{:}\eta^2\text{-}C_2R)$, which readily transform into the $48e^-$ diyne clusters $Ru_3(CO)_7(\mu\text{-}\eta^2\text{-}Ph_2PC_2CCR)$, as a result of acetylide ligand coupling. Reaction sequences and solution spectroscopic data are discussed, and the structural details of seven clusters are described [59]. The thermal decomposition of $Ru_3(CO)_{10}$(dppe) in refluxing benzene has been studied. The cluster complexes $Ru_4(CO)_9(\mu\text{-}CO)(\eta^4\text{-}\mu_4\text{-}C_6H_4)(\eta^2\text{-}\mu_1{:}\mu_4\text{-}PCH_2CH_2PPh_2)$ and $Ru_3(CO)_9(\eta^2\text{-}\mu_1{:}\mu_2\text{-}C_6H_5)(\eta^3\text{-}\mu_1{:}\mu_2\text{-}PPhCH_2CH_2PPh_2)$ have been isolated and characterized in solution by IR and NMR (1D and 2D techniques) spectroscopies, and X-ray diffraction analysis in the case of the former product, where a square-planar Ru_4 skeleton containing an $\eta\text{-}\mu_4$-benzyne ligand and a an $\eta^2\text{-}\mu_1{:}\mu_4$-phosphinidene-phosphine moiety was confirmed. The reactivity of the dppe ligand in this triruthenium cluster is contrasted with the analogous dppm-substituted cluster $Ru_3(CO)_{10}$(dppm), which affords different thermolysis products [60]. Both C–H and P–Ph bond activations have been verified in the thermolysis of $Ru_3(CO)_{10}$(dppe). The major product found from the reaction conducted in refluxing toluene is $Ru_4(CO)_9(\mu\text{-}CO)[\mu_4\text{-}\eta^2\text{-}PCH_2CH_2PPh_2](\mu_4\text{-}\eta^4\text{-}C_6H_4)$, whose structure was ascertained by X-ray analysis. VT NMR data have confirmed the presence of three independent dynamic processes involving benzyne ligand rotation, CO scrambling, and a twisting movement of the CH_2CH_2 chain. Line-shape analysis of the benzyne motion was achieved and the kinetic parameters for benzyne rotation have been determined. Thermolysis of the related cluster $Ru_3(CO)_{10}$(dfppe) indicates that fluorination of the phenyl rings leads to enhanced ligand stability. No thermal degradation of the ancillary diphosphine ligand was observed in this latter cluster under conditions where the dppe derivative readily undergoes ligand activation [61]. Cluster condensation has been found when $Os_3(CO)_9(\mu\text{-}SbPh_2)(\mu\text{-}H)(\mu_3\text{-}\eta^2\text{-}C_6H_4)$ is treated with alkenes and dienes. The clusters $Os_5(CO)_{14}(\mu_4\text{-Sb})(\mu\text{-}SbPh_2)(\mu\text{-}H)_2(\mu_3\text{-}\eta^2\text{-}C_6H_4)(\mu\text{-}\eta^2\text{-}C_6H_4)$ and $Os_5(CO)_{14}(\mu_4\text{-Sb})(\mu\text{-}SbPh_2)(\mu\text{-}H)(\mu_3\text{-}\eta^6\text{-}C_6H_4)(Ph)$ have been isolated and fully characterized in solution and their molecular structures determined. Treatment of the former Os_5 cluster with various Group 15 ligands leads to the corresponding mono-substituted derivatives, of which the PPh_3-substituted cluster has been structurally characterized [62]. C–C bond coupling of the phenylene ligand with terminal alkynes has been observed when $Os_3(CO)_9(\mu\text{-}SbPh_2)(\mu\text{-}H)(\mu_3\text{-}\eta^2\text{-}C_6H_4)$ is treated with either PhCCH or ^{t}BuCCH. The starting phenylene-substituted cluster has also been found to serve as an effective catalyst for the cyclotrimerization of diphenylacetylene. The X-ray structures of $Os_3(CO)_7(\mu\text{-}SbPh_2)[\mu\text{-}\eta^2{:}\eta^4\text{-}PhC{=}C(H)C_6H_4][\mu\text{-}\eta^1{:}\eta^2\text{-}CH{=}C(H)Ph]$, $Os_3(CO)_9(\mu\text{-}SbPh_2)(\mu_3\text{-}\eta^2\text{-}C_2Bu^t)$, $Os_5(CO)_{14}(\mu_4\text{-Sb})(\mu\text{-}SbPh_2)(\mu\text{-}H)[\mu\text{-}\eta^1{:}\eta^2\text{-}PhC{=}C(H)Bu^t](\mu\text{-}\eta^3\text{-}C_6H_4)$, and $Os_3(CO)_7(\mu\text{-}SbPh_2)[\mu\text{-}\eta^2\text{-}PhC{=}C(H)Ph](\mu\text{-}\eta^3\text{-}C_6H_4)$ are included in this report [63]. PPh_3 addition to $Os_3(CO)_9(\mu\text{-}SbPh_2)(\mu\text{-}H)(\mu_3\text{-}\eta^2\text{-}C_6H_4)$ furnishes $Os_3(CO)_9(PPh_3)(\mu\text{-}SbPh_2)(\mu\text{-}H)(\mu_2\text{-}\eta^2\text{-}C_6H_4)$, which can lose CO, coupled with phenylene recoordination to give $Os_3(CO)_8(PPh_3)(\mu\text{-}SbPh_2)(\mu\text{-}H)(\mu_3\text{-}\eta^2\text{-}C_6H_4)$, or isomerize and deorthometalate to give $Os_3(CO)_9(PPh_3)(\mu\text{-}SbPh_2)(Ph)$. Alternatively, use of excess PPh_3 leads to the new cluster $Os_3(CO)_8(PPh_3)_2(\mu\text{-}SbPh_2)(Ph_2PC_6H_4)$. A crossover study using the *p*-tolyl derivative $Os_3(CO)_9[P(p\text{-tol})_3](\mu\text{-}H)(\mu\text{-}SbPh_2)(\mu_2\text{-}\eta^2\text{-}C_6H_4)$ with excess PPh_3 reveals that the orthometalation reaction involves the activation of the coordinated $P(p\text{-tol})_3$ ligand and not the incoming PPh_3 ligand. The structural features of eight clusters are discussed, with the X-ray structure of $Os_3(CO)_9(PPh_3)(\mu\text{-}SbPh_2)(\mu\text{-}H)(\mu_2\text{-}\eta^2\text{-}C_6H_4)$ shown in Fig. 6 [64].

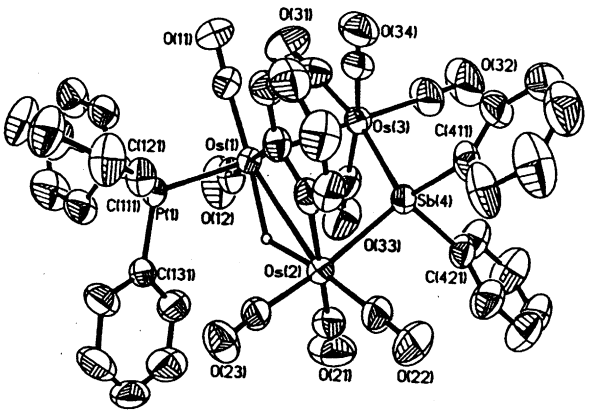

Fig. 6. X-ray structure of $Os_3(CO)_9(PPh_3)(\mu\text{-}SbPh_2)(\mu\text{-}H)(\mu_2\text{-}\eta^2\text{-}C_6H_4)$. Reprinted with permission from Organometallics. Copyright 2002 American Chemical Society.

Phosphine selenides $R_2R'PSe$ (where R = Ph, R′ = Ph, CH_2Ph; R=R′=C_6H_4OMe-4) undergo reaction with $Ru_3(CO)_{12}$ to produce the monoselenide clusters $Ru_3(CO)_7(\mu_3\text{-}CO)(\mu_3\text{-}Se)(PR_2R')_2$ and the bis-selenide-capped clusters $Ru_3(CO)_7(\mu_3\text{-}Se)_2(PR_2R')$. The report describes the X-ray structure of $Ru_3(CO)_7(\mu_3\text{-}CO)(\mu_3\text{-}Se)(PPh_3)_2$, which represents the first structurally characterized Ru_3 cluster that is capped by μ_3-CO and μ_3-Se moieties [65]. The reactivity of 2-mercapto-1-methylimidazole with the cluster complexes $Os_3(CO)_{10}(MeCN)_2$, $Ru_3(CO)_{12}$, $(\mu\text{-}H)Os_3(CO)_8[Ph_2PCH_2P(Ph)C_6H_4]$, $Os_3(CO)_{10}(\mu\text{-dppm})$, and $Ru_3(CO)_{10}(\mu\text{-dppm})$ has been examined. The first two clusters undergo substitution to give $(\mu\text{-}H)Os_3(CO)_{10}[\mu\text{-}SC{=}NCH{=}CHN(Me)]$ and $(\mu\text{-}H)Ru_3(CO)_9[\mu_3\text{-}\eta^2\text{-}SC{=}NCH{=}CHN(Me)]$, respectively. The two phosphine-substituted triosmium clusters both give $(\mu\text{-}H)Os_3(CO)_8[\mu\text{-}SC{=}NCH{=}CHN(Me)](\mu\text{-dppm})$ at elevated temperatures. The same heterocyclic ligand reacts with $Ru_3(CO)_{10}(\mu\text{-dppm})$ to furnish the known cluster $Ru_3(CO)_7(\mu_3\text{-}CO)(\mu_3\text{-}S)(\mu\text{-dppm})$. The molecular structures of the first three products have been determined and their structural similarities are discussed. The reactivity of the 2-mercapto-1-methylimidazole with these clusters is contrasted with the known substitution reactions exhibited by other heterocycles [66]. Treatment of the unsaturated cluster $Os_3(CO)_9[\mu_3\text{-}\eta^2\text{-}C_7H_3(2\text{-Me})NS](\mu\text{-}H)$ with excess diazomethane gives the cluster $Os_3(CO)_9[\mu\text{-}\eta^2\text{-}C_7H_3(2\text{-Me})NS](\mu\text{-}CH_2)Me$, which represents a rare example of an Os_3 complex possessing an edge-bridged methylene moiety and a σ-bound methyl group. Thermolysis of the latter cluster gives $Os_3(CO)_9[\mu_3\text{-}\eta^2\text{-}CHC_7H_3(2\text{-Me})NS](\mu\text{-}H)_2$ and $Os_3(CO)_8[\mu_3\text{-}\eta^2\text{-}CC_7H_3(2\text{-Me})NS](\mu\text{-}H)_3$. The related cluster $Os_3(CO)_9(\mu_3\text{-}\eta^2\text{-}C_7H_4NS)(\mu\text{-}H)$ reacts with diazomethane under similar conditions to produce $Os_3(CO)_9(\mu_3\text{-}\eta^2\text{-}CHC_7H_4NS)(\mu\text{-}H)_2$, which upon thermolysis affords $Os_3(CO)_8(\mu_3\text{-}\eta^2\text{-}CC_7H_4NS)(\mu\text{-}H)_3$. The substitution pattern associated with the bound heterocycle is discussed relative to the CH_2 activation sequence. The two X-ray structures that accompany this report are fully discussed [67]. New mixed Sb/Se and Sb/Te triiron clusters have been prepared and structurally characterized. The dianions $[Fe_3(CO)_9(\mu_3\text{-E})]^{2-}$ (where E = Se, Te) react with MesSbBr to give $Fe_3(CO)_9(\mu_3\text{-E})(\mu_3\text{-SbMes})$. Both clusters exhibit a *nido* core containing a square pyramidal FeSbFeE unit that is capped by an $Fe(CO)_3$ fragment, as confirmed by X-ray crystallography. The related cluster $Fe_3(CO)_{10}(\mu_3\text{-}\eta^2{:}\eta^1\text{-SeSbMes})$ was also isolated and structurally characterized [68].

$H_4Ru_4(CO)_{12}$ has been allowed to react with 1-penten-3-yne to yield the cluster products $Ru_4(CO)_{10}(\mu\text{-CO})(\mu_4\text{-}\eta^1{:}\eta^2{:}\eta^1{:}\eta^2\text{-}C_5H_6)_2$, $Ru_4(CO)_8(\mu_4\text{-}\eta^4{:}\eta^1{:}\eta^1{:}\eta^1{:}\eta^3\text{-}C_{10}H_{12})(\mu_3\text{-}\eta^3{:}\eta^2{:}\eta^1\text{-}C_5H_6)$, and $Ru_4(CO)_{10}(\mu_4\text{-}\eta^4{:}\eta^1{:}\eta^1{:}\eta^3{:}\eta^1\text{-}C_{15}H_{16})$, which are formed as a result of alkyne dimerization and trimerization. These products have been characterized by IR and NMR (^1H and ^{13}C) spectroscopies, and the molecular structures of the first two products have been determined by X-ray crystallography [69]. A rational synthesis for the preparation of tetraruthenium polyhydride clusters has been published. Hydride reduction of $CpRuCl_2(\eta^3\text{-allyl})$ by $LiAlH_4$, followed by work-up in a protic solvent, furnishes the cluster $Cp_4Ru_4H_6$. This same method may be used to produce the related cyclopentadienyl derivatives $(MeCp)_4Ru_4H_6$ and $(\eta^5\text{-}1,3\text{-}Me_2C_5H_3)_4Ru_4H_6$, when the requisite allyl-substituted starting material is employed. The mixed Cp complexes $Cp_{4-x}Cp^*_xRu_4H_6$ (where $x = 1, 2, 3$) are easily synthesized through a minor modification of the original synthesis. T_1 spin-lattice relaxation measurements on the hydride signal in $Cp_4Ru_4H_6$ indicate that the hydrides exist as classical Ru–H units with no bonding between the hydrogen atoms. Three X-ray structures, which all exhibit a Ru_4 tetrahedral core, accompany this report. The important structural details inherent in each cluster are discussed [70]. The role of in situ formed polynuclear aggregates in the hydrosilation of alkynes is described. Treatment of $RuH(XY)(CO)(PR_3)_2$ (where XY = Cl, acac, AcO) with Et_3SiH and phenylacetylene yields a Ru_4 intermediate, which has been structurally characterized by X-ray analysis in the case of $RuH(Cl)(CO)(^iPr_3P)_2$ and its reaction with Et_3SiH [71]. A paper describing carbon-chain formation on metallic arrays has appeared. The open, planar clusters $Ru_4(\mu_4\text{-}C_2)Cp_2(\mu\text{-CO})_2(CO)_8$ (where Cp = Cp, MeCp) react with added dmad to furnish several products, of which $Ru_4[C_2C(CO_2Me)C(CO_2Me)]Cp_2(CO)_9$, $Ru_4[\mu_4\text{-}CCC(CO_2Me)C(CO_2Me)]Cp_2(\mu\text{-CO})(CO)_8$, and $[CpRu(CO)_2]_2[\mu\text{-}CCC(CO_2Me){=}C(CO_2Me)C(O)]$ have been isolated and fully characterized by FAB mass spectrometry, and IR and NMR (^1H and ^{13}C) spectroscopies. The X-ray crystal structures of three complexes are presented, and the sequence involving the dmad insertion reaction is discussed relative to other alkyne insertion pathways [72].

The addition of $Os(CO)_4(CNBu^t)$ to $Os_3(CO)_{12}X_2$ (where X = Cl, Br) at 60 °C leads to the formation of the pentaosmium clusters $(^tBuNC)X(OC)_3OsOs_3(CO)_{12}Os(CO)_3(CNBu^t)X$. X-ray analysis of the chloro derivative

exhibits a linear chain of five osmium atoms. The UV-Vis spectral properties of these Os_5 clusters are compared to analogous Os_4, Os_3, Os_2 derivatives [73]. The aminophosphinidene cluster $Ru_5(CO)_{15}(\mu_4\text{-}PNPr^i_2)$ reacts with added $[PPN][NO_2]$ to give the mixed nitrosyl-phosphinidene cluster $[PPN][Ru_5(CO)_{13}(\mu\text{-}NO)(\mu_4\text{-}PNPr^i_2)]$. Treatment of this product with triflic acid leads to the nitrene-capped cluster $Ru_5(CO)_{10}(\mu\text{-}CO)_2(\mu_3\text{-}CO)(\mu_4\text{-}NH)(\mu_3\text{-}PNPr^i_2)$. The molecular structures of these products have been determined. $[PPN][Ru_5(CO)_{13}(\mu\text{-}NO)(\mu_4\text{-}PNPr^i_2)]$ contains 74 valence electrons and exhibits a *nido* Ru_5 core or a *closo* Ru_5P polyhedron when the $\mu_4\text{-}PNPr^i_2$ unit is included in the cluster core. The nitrene-capped cluster also contains 74 valence electrons and a square-based pyramidal structure that is consistent with electron-precise bonding rules [74]. A detailed report on the reaction between $Ru_5(CO)_{15}(\mu_4\text{-}PNPr^i_2)$ and $[PPN][NO_2]$ has been published. Treatment of $[PPN][Ru_5(CO)_{13}(\mu_2\text{-}NO)(\mu_4\text{-}PNPr^i_2)]$ with $HBF_4{\cdot}Et_2O$ gives a mixture of $Ru_5(CO)_{13}(\mu_5\text{-}N)[\mu_2\text{-}P(F)NPr^i_2]$ and $Ru_5(CO)_{10}(\mu\text{-}CO)_2(\mu_3\text{-}CO)(\mu_4\text{-}NH)(\mu_3\text{-}PNPr^i_2)$. When the same anionic Ru_5 cluster is allowed to react with CF_3SO_3Me, $Ru_5(CO)_{13}(\mu_5\text{-}N)[\mu_2\text{-}P(OMe)NPr^i_2]$ is observed as the sole product. The molecular structures of four products have been solved and discussed. A working reaction mechanism illustrating the different Ru_5 intermediates and their reactivity towards the various acids and electrophiles used are presented [75]. The redox properties of the face-coordinated C_{60}-carbidopentaruthenium clusters $Ru_5C(CO)_{11}(PPh_3)(\mu_3\text{-}\eta^2\text{:}\eta^2\text{:}\eta^2\text{-}C_{60})$, $Ru_5C(CO)_{10}(\mu\text{-}\eta^1\text{:}\eta^1\text{-dppf})(\mu_3\text{-}\eta^2\text{:}\eta^2\text{:}\eta^2\text{-}C_{60})$, and $PtRu_5C(CO)_{11}(\eta^2\text{-dppe})(\mu_3\text{-}\eta^2\text{:}\eta^2\text{:}\eta^2\text{-}C_{60})$ have been investigated by CV, RDE voltammetry, and DPV methods. The appropriate non-C_{60}-substituted clusters were also examined, and these data are contrasted with the C_{60}-substituted derivatives. The ability of the C_{60} ligand to function as a reduction site is discussed [76]. Multiple addition of Ph_3SnH to $Ru_5(\mu_5\text{-}C)(CO)_{12}(C_6H_6)$ gives the new clusters $Ru_5(\mu_5\text{-}C)(CO)_8(\mu\text{-}SnPh_2)_4(C_6H_6)$ and $Ru_5(\mu_5\text{-}C)(CO)_7(\mu\text{-}SnPh_2)_4(SnPh_3)(C_6H_6)(\mu\text{-}H)$ in low yields. Both products contain a square pyramidal Ru_5 cluster that possesses an interstitial carbide ligand [77]. UV irradiation of $Ru_5(\mu_5\text{-}C)(CO)_{15}$ in the presence of Ph_3SnH promotes Sn–H bond activation and cleavage of one Ru–Ru bond to produce $Ru_5(\mu_5\text{-}C)(CO)_{15}(SnPh_3)(\mu\text{-}H)$. Thermolysis of the same reactants at 127 °C gives $Ru_5(\mu_5\text{-}C)(CO)_{10}(SnPh_3)(\mu\text{-}SnPh_2)_4(\mu\text{-}H)$, where each ruthenium atom in the square-pyramidal core is bridged by one of $SnPh_2$ ligands. Heating $Ru_5(\mu_5\text{-}C)(CO)_{12}(C_6H_6)$ with added Ph_3SnH at 68 °C yields $Ru_5(\mu_5\text{-}C)(CO)_{11}(C_6H_6)(SnPh_3)(\mu\text{-}H)$ (Fig. 7) and $Ru_5(\mu_5\text{-}C)(CO)_{10}(C_6H_6)(SnPh_3)_2(\mu\text{-}H)_2$ as the isolable products. The molecular structures of these two clusters exhibit square pyramidal Ru_5 polyhedra. The benzene-substituted cluster $Ru_5(\mu_5\text{-}C)(CO)_{12}(C_6H_6)$ reacts with Ph_3SnH at higher temperatures to furnish $Ru_5(\mu_5\text{-}C)(CO)_8(\mu\text{-}SnPh_2)_4(C_6H_6)$ and $Ru_5(\mu_5\text{-}C)(CO)_7(\mu\text{-}SnPh_2)_4(SnPh_3)(C_6H_6)(SnPh_3)(\mu\text{-}H)$. The loss of benzene

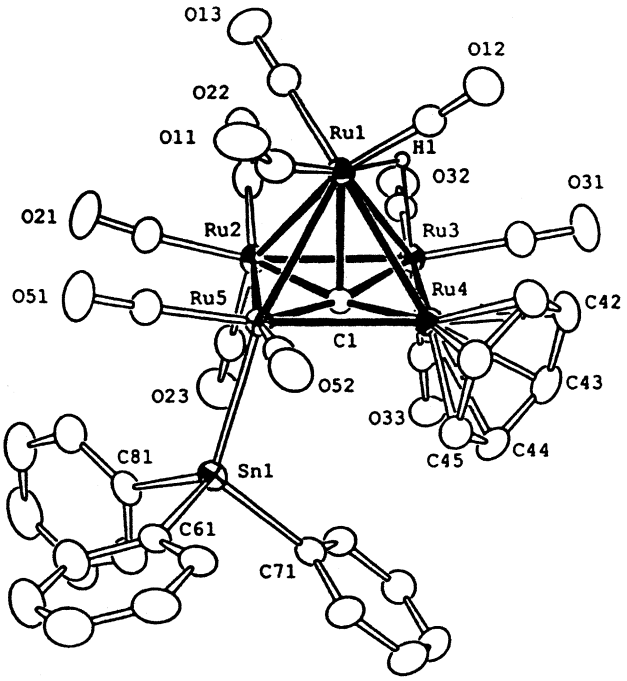

Fig. 7. X-ray structure of $Ru_5(\mu_5\text{-}C)(CO)_{11}(C_6H_6)(SnPh_3)(\mu\text{-}H)$. Reprinted with permission from Inorganic Chemistry. Copyright 2002 American Chemical Society.

and the migration of a phenyl group from a tin ligand to the carbide moiety in $Ru_5(\mu_5\text{-}C)(CO)_{11}(C_6H_6)(SnPh_3)(\mu\text{-}H)$ occurs at 68 °C to give the new cluster $Ru_5(\mu_3\text{-}CPh)(CO)_{11}(C_6H_6)(\mu_4\text{-}SnPh)$. The presence of the quadruply bridged stannylyne ligand has been verified by X-ray diffraction analysis [78].

A report describing the use of the spherical harmonic model in the analysis of bridging CO vibrations in over 100 metal cluster compounds has been published. The sensitivity of the bridging CO groups to the molecular geometry of the cluster within the SHM treatment, as compared to terminal CO groups, is discussed [79]. CH and PC bond activations in PMe_2Ph ligands coordinated to Ru_6 clusters have been documented. Treatment of $Ru_6(CO)_{17}(\mu_6\text{-}C)$ with PMe_2Ph gives an isomeric mixture of $Ru_6(CO)_{15}(PMe_2Ph)_2(\mu_6\text{-}C)$. NMR measurements reveal a slow interconversion between the 1,2-P_2 and the 1,3-P_2-substituted isomers. These isomers react with added Me_3NO at room temperature to furnish the new clusters $Ru_6(CO)_{13}(\mu\text{-}PMe_2)(\mu_3\text{-}\eta^3\text{-}Me_2PC_6H_4)(\mu_6\text{-}C)$ and $Ru_6(CO)_{14}(PMe_2Ph)(\mu\text{-}\eta^2\text{-}MePhPCH_2)(\mu_6\text{-}C)(\mu\text{-}H)$. X-ray diffraction analysis of the former product confirms the presence of a $\mu_2\text{-}PMe_2$ ligand and an orthometalated phenyl moiety that is derived from the ancillary phosphine ligand. The molecular structure of the latter product reveals that one of the methyl groups belonging to the phosphine ligand has undergone a C–H bond activation to give the $3e^-$ bridging ligand CH_2PMePh. Thermolysis of the bisphosphine-substituted clusters affords the aforementioned $\mu_2\text{-}PMe_2$ clus-

ter, in addition to the three new ligand-activated Ru_6 clusters $Ru_6(CO)_{14}(\mu\text{-}PMe_2)(\mu\text{-}\eta^2\text{-}MePhPCH_2)(\mu_6\text{-}C)$, $Ru_6(CO)_{12}(\mu\text{-}PMe_2)(\mu_3\text{-}\eta^2\text{-}C_6H_4)(\mu_6\text{-}C)$, and $Ru_6(CO)_{14}(\mu\text{-}PMe_2)(\mu\text{-}\eta^2\text{-}Me_2PC_6H_4)(\mu_6\text{-}C)$. The molecular structures of these three products all exhibit octahedral Ru_6 cores [80]. The cluster dication $[(\eta^6\text{-}C_6H_6)_2(\eta^6\text{-}C_6Me_6)_4Ru_8(\mu_2\text{-}H)_2(\mu_3\text{-}O)_2(\mu_2\text{-}Cl)_2]^{2+}$ has been synthesized from $[(\eta^6\text{-}C_6H_6)(\eta^6\text{-}C_6Me_6)_2Ru_3(\mu_2\text{-}H)_3(\mu_3\text{-}O)]^+$ and $RuCl_3\cdot H_2O$ in aqueous solution. X-ray diffraction analysis reveals that the cluster is composed of two tetrahedral Ru_4 units that are bound by two chlorine bridging moieties [81].

2.4. Group 9 clusters

The inter- and intramolecular trimerization of alkynes by several alkylidyne-capped tricobalt clusters is reported to give good to excellent yields of benzene derivatives. The trimerization of oct-4-yne by $HCCo_3(CO)_9$ furnishes a near quantitative yield of hexapropylbenzene. The utility of this system is also demonstrated by the construction of a wide variety of polycyclic and spiro-derived benzene compounds [82]. The cluster $(\eta^5\text{-indenyl})_3Ir_3(CO)_3$ reacts with $HBF_4\cdot Et_2O$ to give the corresponding cationic hydride $[(\eta^5\text{-indenyl})_3Ir_3(\mu\text{-}H)(CO)_3]^+$. The cationic cluster is deprotonated by added Et_3N to afford the parent cluster having C_s symmetry. This isomer rapidly transforms into the more stable C_{3v} isomer, which possesses three bridging CO groups. The equilibrium constant for the C_s and C_{3v} isomeric mixture and the activation parameters for the conversion to the CO-bridged isomer have been measured by IR, NMR, and UV-Vis spectroscopies. The ease by which these isomers interconvert is discussed relative to the "indenyl ligand effect" and rotation of an (indenyl)IrCO fragment about an Ir=Ir unit [83]. 2-Mercaptopyridine undergoes reaction with $Co_2(CO)_8$ to produce the sulfido-capped cluster $Co_3(CO)_7(\mu_3\text{-}S)(\mu\text{-}C,N\text{-}C_5H_4N)$; the reaction of this cluster with added Ph_2Ppy to furnishes the bridged cluster $Co_3(CO)_5(\mu_3\text{-}S)[\mu\text{-}C(O),N\text{-}C_5H_4N(C{=}O)](\mu\text{-}P,N\text{-}Ph_2Ppy)$. The carbonylation of the Co–C(pyridyl) bond in the starting cluster and the ligation of the P and N atoms of the ancillary phosphine ligand were confirmed by X-ray analysis. Treatment of $Co_3(CO)_7(\mu_3\text{-}S)(\mu\text{-}C,N\text{-}C_5H_4N)$ with CO leads to $Co_3(CO)_7(\mu_3\text{-}S)[\mu\text{-}C(O),N\text{-}C_5H_4N(C{=}O)]$. The use of 2-quinolinethiol afforded the analogous sulfido-capped cluster $Co_3(CO)_7(\mu_3\text{-}S)(\mu\text{-}C,N\text{-}C_9H_6N)$, which was resistant to carbonylation. Ph_2Ppy coordination to the quinoline-substituted cluster proceeds with formation of $Co_3(CO)_5(\mu_3\text{-}S)(\mu\text{-}C,N\text{-}C_9H_6N)(\mu\text{-}P,N\text{-}Ph_2Ppy)$ as the major product, along with a minor amount of the Co-C(quinoline) carbonylation product. Solution NMR data (^1H–^1H COSY) are presented, and the molecular structures of seven additional clusters are discussed [84]. The reaction of $Rh_2Cl_2(cod)_2$ with the hydrido-hydrogensulfido complex $Cp^*IrH(SH)PMe_3$ gives the compound $Cp^*Ir(PMe_3)(\mu_2\text{-}H)(\mu_3\text{-}S)[Rh(cod)][RhCl(cod)]$ in the presence of Et_3N. Treatment of the bis(hydrogensulfido) compound $Cp^*Ir(SH)_2(PMe_3)$ with $Rh_2Cl_2(cod)_2$ gives the sulfido-capped cluster $Cp^*Ir(\mu_3\text{-}SH)_2[Rh(cod)]_2$. The X-ray structure of this latter cluster consists of a near isosceles $IrRh_2$ triangle where two weak Ir–Rh bonds are present. The absence of any significant Rh–Rh bonding is attributed to the pseudo-square-planar Rh(I) centers, whose high lying p_z orbitals are unavailable for bonding [85]. Heating the iridium dimer $Cp^*Ir(SH)(\mu_2\text{-}SH)_2IrCp^*(SH)$ in benzene leads to the triiridium sulfido-hydrosulfido cluster $(Cp^*Ir)_3(\mu_3\text{-}S)(\mu_2\text{-}S)(\mu_2\text{-}SH)_2$. Treatment of the same dimer with $(Cp^*IrCl)_2(\mu_2\text{-}H)_2$ (0.5 equiv.) or $[Cp^*Ir(\mu_2\text{-}SH)_3IrCp^*]^+$ with added Et_3N produces the related iridium cluster $[(Cp^*Ir)_3(\mu_3\text{-}S)(\mu_2\text{-}SH)_3]^+$. The mixed-metal Ir_2Pd_2 cluster $(Cp^*Ir)_2(SH)(\mu_3\text{-}S)_2[Pd(PPh_3)]_2(\mu_2\text{-}SH)$ has been obtained from the reaction of Pd(dba)/PPh_3 and $Cp^*Ir(SH)(\mu_2\text{-}SH)_2IrCp^*(SH)$. The structures of four complexes have been solved and are discussed [86].

The reaction of $Rh_4(CO)_{12}$ with synthesis gas has been reinvestigated by in situ FT-IR spectroscopy. The formation of $HRh(CO)_4$ was confirmed by using a band-target entropy minimization deconvolution technique, which has allowed for the unequivocal observation and band assignments for this elusive monorhodium compound. The equilibrium constant for the conversion of $HRh(CO)_4$ into $Rh_4(CO)_{12}$ has been determined, and a plausible reaction sequence starting with the aggregation of $HRh(CO)_4$ is discussed [87]. A report on the $Ir_4(CO)_{12}$-catalyzed coupling of imidazoles with aldehydes in the presence of $HSiEt_2Me$ has appeared. The major product that is isolated from this reaction is a 2-substituted imidazole. A reaction mechanism that involves the addition of a transient Ir-alkyl species across the C=N bond of the imidazole substrate is proposed [88]. The application of a band-target entropy minimization (BTEM) algorithm on the recovery of the pure component from a $Rh_4(CO)_{12}/Rh_6(CO)_{16}$ mixture has been described. The utility of this analytical method for the study of in situ spectroscopic data from transition-metal-catalyzed reactions is thoroughly discussed [89]. The homogeneous hydroformylation of 3,3-dimethylbut-1-ene using the catalyst precursor $Rh_4(CO)_{12}$ has been examined by the BTEM technique, which has enabled the IR observation of $RC(O)Rh(CO)_4$ and $Rh_6(CO)_{16}$ under autogeneous catalysis. An all terminal CO isomer of $Rh_4(CO)_{12}$ has also been observed in the reaction solution [90]. The use of $Rh_4(CO)_{12}$ as a catalyst in the hydroformylation of 4-vinylpyridine is described. The effect of added PMe_2Ph on the aldehyde-to-hydrogenation product is discussed, with the hydrogenation product, 4-ethylpyridine, being favored with increasing substrate concentration and substrate conversion. Deuterioformylation studies confirm the origin of the 4-ethylpyridine as arising from the cleavage of the Rh–carbon bond of the branched Rh-alkyl intermediate by the acidic proton from the enol derived from the product aldehyde [91]. Propiolic acid has been allowed to react with $Co_4(CO)_{12}$ to give the corresponding alkyne-substituted *closo*-Co_4C_2 cluster. The X-ray structure of the product contains a C(1)–C(2)–C(3) fragment

that is half way between acrylic and acetylene-carboxylic acids. The thermal stability of $Co_4(CO)_{10}(HC_2CO_2H)$ has been explored by thermogravimetric analysis, where heating promotes decomposition to give phases containing a high cobalt content. The redox chemistry of this Co_4 cluster has been examined by cyclic voltammetry, with the redox data being discussed relative to Fenske–Hall MO calculations [92]. The synthesis and molecular structure of $Co_4(CO)_{10}(\mu\text{-CO})[H_2C{=}CC(Me)_2N(Me)C(Me)_2(\mu_4\text{-C})]$, which is obtained from the reaction of $Co_4(CO)_{12}$ with $(HC_2CMe_2)_2NMe$, have been published. The structure exhibits a "spiked triangular" array of four cobalt atoms that is bound by a $6e^-$ acetylide moiety [93]. 1-Alkynes are readily coordinated by the mixed-metal cluster $Co_2Rh_2(CO)_{12}$ to give the *closo*-$Co_2Rh_2C_2$ octahedral clusters. Spectroscopic and structural data indicate that the alkyne ligand undergoes insertion regioselectively into the Co–CO bond. The reactivity of alkynes with $Co_3Rh(CO)_{12}$ is also reported [94]. The redox properties of the tetracobalt clusters $Co_4(CO)_3(\mu_3\text{-CO})_3(\mu_3\text{-}C_8H_8)L_2$ (where $L_2 = \eta^4\text{-}C_8H_8$, $\eta^4\text{-}C_6H_8$, η^4-6,6-$Ph_2C_6H_4$) that contain a facially coordinated cot ligand have been explored by cyclic voltammetry, dropping mercury electrode polarography, and controlled potential coulometry. The electrochemical results are discussed with respect to DFT MO calculations. The stability of the electrochemically generated radical anions is shown to be modulated by the ancillary cot ligand [95]. New monomeric and linked cobalt clusters containing a *closo*-Si_2Co_4 core have been synthesized. $PhSiH_3$ reacts with $Co_4(CO)_{12}$ to afford the $64e^-$ cluster $Co_4(CO)_{11}(\mu_4\text{-SiPh})_2$. The X-ray structure confirms the pseudo-octahedral Co_4Si_2 core and the presence of the μ_4-SiPh moieties. The dimeric cluster $[Co_4(CO)_{11}(\mu_4\text{-SiPh})Si]_2C_6H_4$ has been synthesized from $PhSiH_3$, $H_3SiC_6H_4SiH_3$, and $Co_4(CO)_{12}$. Related dimers containing a $-(CH_2)_8-$ spacer group have also been synthesized and characterized in solution. Electrochemical studies employing cyclic and square wave voltammetries reveal that each Co_4Si_2 core undergoes a one-electron reduction and that there in no electronic communication between the Co_4Si_2 cores in the dimeric compounds [96]. Ligand substitution in $HIr_4(CO)_{10}(\mu\text{-}PPh_2)$ with the ligands PMe_3, PPh_3, dppm, dppe, dppb, and (*Z*)-$Ph_2PCH{=}CHPPh_2$ has been studied. With PMe_3, both $HIr_4(CO)_9(PMe_3)(\mu\text{-}PPh_2)$ and $HIr_4(CO)_8(PMe_3)_2(\mu\text{-}PPh_2)$ have been isolated from the reaction, with two isomers of the former cluster observed in solution, whose interconversion involves an intramolecular migration of the PMe_3 ligand about the cluster polyhedron. No kinetic isomers were observed in $HIr_4(CO)_9(PPh_3)(\mu\text{-}PPh_2)$. The nature of the substitution product(s) with the diphosphine ligands is shown to depend on the size of the length of the carbon chain. Structures are proposed for all compounds, on the basis of ^1H and ^{31}P NMR data, coupled with spectral correlations already established for phosphine and diphosphine derivatives of $Ir_4(CO)_{12}$. Three X-ray structures have been determined and their structural features discussed [97]. The intramolecular dynamics for CO and phosphido ligand scrambling in $Rh_4(CO)_6(\mu\text{-}PPh_2)_4$ have been studied by using ^{103}Rh, ^{31}P, and ^{13}C NMR measurements. The activation parameters for ^{31}P and ^{13}C exchange have been determined by ^{31}P and ^{13}C EXSY spectroscopy [98].

Tripyrrolylphosphine reacts with $Rh_6(CO)_{15}(MeCN)$ to initially give $Rh_6(CO)_{15}[\eta^1\text{-}P(NC_4H_4)_3]$, followed by CO loss and nitrogen coordination to produce $Rh_6(CO)_{14}[\mu\text{-}P(NC_4H_4)_3]$. X-ray structural data reveal that the phosphine ligand bridges adjacent rhodium centers through the phosphine moiety and one of the pyrroyl nitrogen groups. Solution NMR measurements indicate that the phosphine ligand is not statically bound to the Rh_6 core and participates in three distinct dynamic processes. The results of ^1H TOCSY and EXSY experiments are discussed relative to the mechanism proposed for the fluxional behavior. The cluster $Rh_6(CO)_{14}[\mu\text{-}P(NC_4H_4)_3]$ undergoes reaction with CO to regenerate $Rh_6(CO)_{15}[\eta^1\text{-}P(NC_4H_4)_3]$. The carbonylation kinetics for the forward and reverse reaction have been measured, and the Van't Hoff data and the activation parameters are reported. The intrinsic entropy of the bidentate-bridged cluster is exceptionally unfavorable, which facilitates CO addition and the reversibility of this reaction [99]. Treatment of $Ir_6(CO)_{16}$ with excess cycloheptatriene in refluxing toluene furnishes $Ir_6(CO)_{13}(C_7H_8)$. X-ray analysis confirms that the Ir_6 core consists of an octahedron, where one Ir_3 is capped by the $\mu_3\text{-}\eta^2{:}\eta^2{:}\eta^2$-cycloheptatriene ligand (Fig. 8). This cluster is deprotonated by Na_2CO_3 in THF to give $[Ir_6(CO)_{12}(C_7H_7)]^-$, which contains a planar cycloheptatrienyl ligand. The neutral product undergoes a two-electron reduction that is accompanied by decarbonylation to give $[Ir_6(CO)_{12}(C_7H_8)]^{2-}$. The dianion exhibits a two-electron oxidation, which after deprotonation gives the aforementioned monoanion [100].

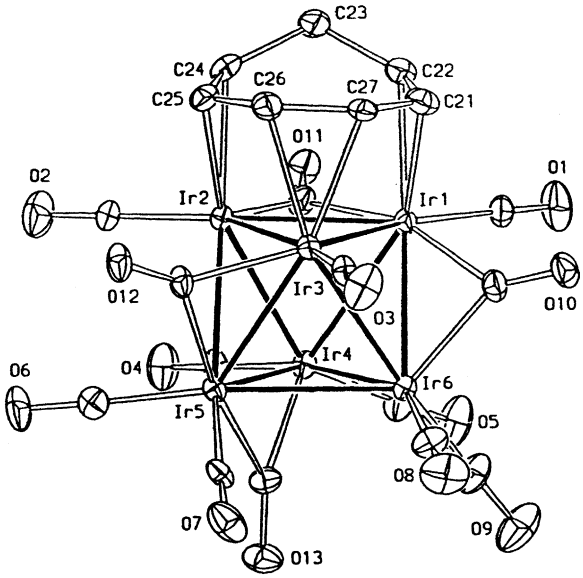

Fig. 8. X-ray structure of $Ir_6(CO)_{13}(\mu_3\text{-}\eta^2{:}\eta^2{:}\eta^2\text{-}C_7H_8)$. Reprinted with permission from Organometallics. Copyright 2002 American Chemical Society.

A report discussing the topologies available to polynuclear iridium clusters containing fused octahedra and trigonal pyramids has appeared. The bonding patterns exhibited by $[Ir_9(CO)_{20}]^{3-}$, $[Ir_{10}(CO)_{21}]^{2-}$, $[Ir_{11}(CO)_{23}]^{3-}$, $[Ir_{12}(CO)_{24}]^{2-}$, and $[Ir_{14}(CO)_{27}]^{-}$ are fully discussed [101].

2.5. Group 10 clusters

The activation of C–H bonds in internal alkenes and dienes is achieved by treatment of nickelocene with added sodium. The in situ generated "CpNi" dehydrogenates the internal alkenes to alkynes, which then react with the "CpNi" intermediate to produce the alkyne complex $(CpNi)_3(RC_2R)$. When a methyl group is adjacent to the alkene linkage, the tetrahedrane clusters $(CpNi)_3CR$ may be isolated from the reaction. Use of 1,5-hexadiene with Cp_2Ni/Li affords the alkylidyne-capped cluster $(CpNi)_3CCH_2CH_2CH_2CH{=}CH_2$ and the intramolecular chelate compound $CpNiCH(Me)CH_2CH_2CH{=}CH_2$. Also, found in these reactions in varying yields are $(CpNi)_2CpH$ and $(CpNi)_4H_4$. The X-ray structure of $(CpNi)_3$(3-hexyne) is presented and discussed [102]. The reaction of $Pt_2(\mu\text{-}Se)_2(PPh_3)_4$ with $PtCl_2$(cod) gives the expected trinuclear cluster $[Pt_2(\mu_3\text{-}Se)_2(PPh_3)_4\{Pt(cod)\}]^{2+}$, along with the unexpected bis(cod)-substituted cluster $[Pt(\mu_3\text{-}Se)_2(PPh_3)_2\{Pt(cod)\}_2]^{2+}$. The latter cluster arises from a metal scrambling process, which has been unequivocally demonstrated by electrospray mass spectrometry [103]. The triangular clusters $Pt_3(\mu\text{-}CO)_3(PR_3)_3$ react with hexafluoro-2-butyne via fragmentation to give the diplatinum complexes $Pt_2(CO)_2(PR_3)_2(\mu\text{-}\eta^2{:}\eta^2\text{-}CF_3C_2CF_3)$ [104]. The redox properties of $[Pd_3(dppm)_3(CO)I]^{2+}$ have been explored by CV, RDE voltammetry, and coulometric methods. The overall observed $2e^-$ reduction is shown to proceed by simultaneous EEC and ECE steps. In the former sequence, there are two sequential one-electron reductions, followed by iodide loss to give $Pd_3(dppm)_3(CO)$; the latter manifold reveals a one-electron reduction, followed by iodide elimination and a second one-electron reduction step, to furnish the same neutral Pd_3 cluster. Control over these competitive mechanisms is achieved by changing the temperature, solvent polarity, iodide concentration, and sweep rate. The overall electrochemical results were successfully simulated by using a six-membered square scheme [105]. Capping of the Pt_3 face in $[Pt_3(\mu_3\text{-}CO)(\mu\text{-}dppm)_3]^{2+}$ by Tl(acac) gives $[Pt_3\{\mu_3\text{-}Tl(acac)(H_2O)\}(\mu_3\text{-}CO)(\mu\text{-}dppm)_3]^{2+}$. The thallium(I) moiety is readily replaced by halides, acetate, and $SnCl_3^-$ to give $[Pt_3(\mu_3\text{-}CO)(\mu_3\text{-}X)(\mu\text{-}dppm)_3]^{+}$. The X-ray structures of two Pt_3Tl clusters are reported, with each Pt_3Tl frame shown to exhibit a tetrahedral core [106]. The dinuclear complexes $(C_6F_5)_2Pt(\mu\text{-}PPh_2)_2Pt(PPh_2R)_2$ (where R = Ph, Me, Et) react with Pt(2-norbornene)$_3$ to produce the triangular clusters $Pt_3(\mu\text{-}PPh_2)_2(\mu\text{-}C_6F_5)(C_6F_5)(PPh_2R)_2$, which contain two bridging phosphido ligands and one bridging pentafluorophenyl moiety. All three clusters possess 42 valence electrons. Treatment of the PPh_3 derivative with $AgClO_4$ and $Ag(OClO_3)(PPh_3)$ gives $Pt_3(AgOClO_3)(\mu\text{-}PPh_2)_2(\mu\text{-}C_6F_5)(C_6F_5)(PPh_3)_2$ and $[Pt_3Ag(\mu\text{-}PPh_2)_2(\mu\text{-}C_6F_5)(C_6F_5)(PPh_3)_3][ClO_4]$, respectively. ^{31}P and ^{19}F NMR data and two X-ray structures are presented and discussed [107]. The first example of a triangular $Pt^IPt^IPt^{II}$ cluster containing both ethylene and CO ligands has appeared. Hydride abstraction in $Pt_3(\mu\text{-}PBu^t_2)_3(H)(CO)$ by $[Cp_2Fe][PF_6]$, followed by coordination of CO, affords the symmetrical cluster $[Pt_3(\mu\text{-}PBu^t_2)_3(CO)_3]^{+}$. Use of MeCN or ethylene in place of CO furnishes the corresponding ligand-substituted clusters $[Pt_3(\mu\text{-}PBu^t_2)_3(CO)_2L]^{+}$, with Fig. 9 showing the ethylene-substituted cluster $[Pt_3(\mu\text{-}PBu^t_2)_3(CO)_2(\eta^2\text{-}C_2H_4)]^{+}$. All new complexes have been characterized in solution by ^{31}P and ^{195}Pt NMR spectroscopies, and the simulation of the spectral data have provided accurate chemical shifts and coupling constant information. The molecular structure of the hydrido cluster $[Pt_3(\mu\text{-}PBu^t_2)_3(H)(CNBu^t)_2]^{+}$ accompanies this report [108].

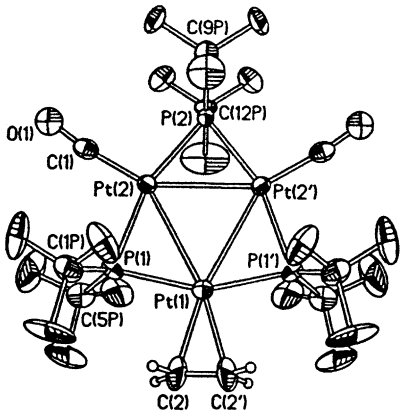

Fig. 9. X-ray structure of $[Pt_3(\mu\text{-}PBu^t_2)_3(CO)_2(\eta^2\text{-}C_2H_4)]^{+}$. Reprinted with permission from Organometallics. Copyright 2002 American Chemical Society.

The unstable ennanuclear nickel cluster $[Ni_9(CO)_{16}]^{2-}$ has been synthesized from the reaction of $[Ni_6(CO)_{12}]^{2-}$ with $Cu(PPh_3)_xCl$ (where $x = 1, 2$) and from the degradation of $[H_2Ni_{12}(CO)_{12}]^{2-}$ by PPh_3. The X-ray structure of the product exhibits a close-packed two-layer metal core geometry, whose similarities are contrasted with other structurally characterized high nuclearity clusters [109].

2.6. Group 11 clusters

The synthesis and photophysical properties of the luminescent tetranuclear silver (I) arylacetylides $Ag_4[\mu\text{-}(CC)_xC_6H_4R\text{-}p](PCy_3)_y$ (where $x = 1$, $y = 2$, R = H, Me, OMe, CCPh; $x = 2$, $y = 4'$ R = H) have been published. Treatment of $Ag_4[\mu\text{-}(CC)_xC_6H_4R\text{-}p]$ with PCy_3 in the absence of light affords the phosphine-substituted Ag_4 clusters. The molecular structure of $Ag_4(\mu\text{-}CCPh)_4(PCy_3)_2$ consists of a planar parallelogram-like Ag_4 core, where the

Ag–Ag separations support a weak bonding interaction between the silver centers. The analysis of the spectroscopic assignments in these Ag_4 clusters is facilitated by the use of PCy_3 as an ancillary ligand, since this ligand does not exhibit low-lying ligand-localized excited states, unlike the previous Ag_4 complexes that have employed triarylphosphine ligands [110].

3. Heterometallic clusters

3.1. Trinuclear clusters

A report on the synthesis and spectroscopic characterization of tetrahedrane clusters possessing functionally bridged dicyclopentadienyl ligands has appeared. Included in this work are the X-ray structures of $[Mo_2Fe(\mu_3\text{-}S)(CO)_7][\eta^5\text{-}C_5H_4C(O)CH_2]_2$, $[W_2Fe(\mu_3\text{-}S)(CO)_7]_2[\{\eta^5\text{-}C_5H_4C(O)CH_2\}_2]_2$, and $[Mo_2Fe(\mu_3\text{-}S)(CO)_7][\eta^5\text{-}C_5H_4CH(OH)CH_2]_2$ [111].

The reaction of $[Mn(CO)_5]^-$ with diorganyl disulfides in the presence of $Co_2(CO)_8$ furnishes the trinuclear complexes $(OC)_4Mn(\mu\text{-}SR)_2Co(CO)(\mu\text{-}SR)_3Mn(CO)_3$. The X-ray structure of the *o*-benzamidophenyl thiol derivative reveals the presence of a linear Mn–Co–Mn linkage [112]. Insertion of the bis(phosphine) fragment $Pt(PPh_3)_2$ into the S–S bond of $Mn_2(CO)_7(\mu\text{-}S_2)$ affords the corresponding five-vertex *arachno* cluster $Mn_2(CO)_7(\mu_3\text{-}S)_3Pt(PPh_3)_2$. Loss of CO gives the hexacarbonyl cluster $Mn_2(CO)_6(\mu_3\text{-}S)_3Pt(PPh_3)_2$, which has been shown by X-ray crystallography to consist of an open Mn_2Pt core with one Mn–Mn bond and one Mn–Pt bond. CO readily adds to this *nido* cluster to regenerate the *arachno* cluster [113]. S–S bond reactivity has been examined in the reaction of $Mn_2(CO)_7(\mu\text{-}S_2)$ with various cyclopentadienylmetal compounds. Use of $CpCo(CO)_2$ and $Cp^*Rh(CO)_2$ in the reaction leads to the triangular Mn_2M clusters $CpCoMn_2(CO)_6(\mu_3\text{-}S)_2$ and $Cp^*RhMn_2(CO)_6(\mu_3\text{-}S)_2$, respectively. Fig. 10 shows the structure of the latter cluster, which exhibits a five-vertex *closo*-$CoMn_2S_2$ polyhedron [114].

The telluride complex $(\eta^5\text{-}^t BuCp)_2Nb(Te_2)H$ has been allowed to react with $Fe_2(CO)_9$ to give $[(\eta^5\text{-}^t BuCp)_2Nb(Te)_2H]Fe_2(CO)_6$, which upon treatment with $Cr(CO)_5(THF)$ produces $[(\eta^5\text{-}^t BuCp)_2Nb(Te)_2H\{Fe_2(CO)_6\}]Cr(CO)_5$ in essentially quantitative yield. The X-ray structure of the $NbFe_2Cr$ cluster and the VT NMR data for both clusters are discussed [115]. The unsaturated 46-electron cluster $Fe_2W(CO)_5Cp[\mu_3\text{-}\eta^2\text{-}(\perp)\text{-}HCCPh](\mu\text{-}CO)(\mu\text{-}PPh_2)$, where an Fe-W edge is perpendicularly bridged by the alkyne molecule, has been isolated from the reaction of $Fe_2(CO)_6(\mu\text{-}\eta^2\text{-}CCPh)$ and $Cp_2W_2(CO)_4$. Use of $Cp_2Mo_2(CO)_4$ gives the analogous unsaturated Fe_2Mo cluster, in addition to the saturated cluster $FeMo_2Cp_2(CO)_5[\mu_3\text{-}\eta^2\text{-}(\perp)\text{-}HCCPh](\mu\text{-}PPh_2)$. The synthesis and characterization of the FeWCo acetylide-bridged cluster $FeWCoCp_2(CO)_6[\mu_3\text{-}\eta^2\text{-}(\perp)\text{-}HCCPh](\mu\text{-}PPh_2)$ is described. Carbonylation studies of the Fe_2Mo 46-electron cluster confirms the existence of a $\perp$ -$\parallel$ alkyne reorientation and formation of the 48-electron cluster $Fe_2Mo(CO)_6Cp[\mu_3\text{-}\eta^2\text{-}(\parallel)\text{-}HCCPh](\mu\text{-}CO)(\mu\text{-}PPh_2)$. This cluster readily loses CO and reverts back to the starting alkyne cluster. The reversible $\perp$ -$\parallel$ alkyne reorientation adheres to expectations in keeping with PSEP theory. The molecular structures of five clusters are presented and their structural highlight are discussed [116]. Thermolysis of $Fe_2Mo(CO)_{10}(\mu_3\text{-}Se)_2$ with added $Cp^*W(CO)_3(CCPh)$ under oxygen leads to $Cp^*MoWFe_2(O)(\mu_3\text{-}Se)(\mu_4\text{-}Se)(CO)_8(CCPh)$, while heating the sulfur-capped derivative $Fe_2Mo(CO)_{10}(\mu_3\text{-}S)_2$ with $Cp^*W(CO)_3(CCPh)$ under argon gives the oxygen-free cluster $Cp^*MoWFe_4(\mu_3\text{-}S)_3(\mu_4\text{-}S)(CO)_{14}(CCPh)$. Carrying out this latter reaction with added oxygen produces $Cp^*WMo_2(\mu\text{-}O)_2(\mu\text{-}S)(\mu_3\text{-}CCPh)[Fe_2(CO)_6(\mu_3\text{-}S)_2]_2$, $Cp^*WMo_2(O)_2(\mu\text{-}O)(\mu\text{-}CCPh)[Fe_2(CO)_6(\mu_3\text{-}S)_2]$, and $Cp^*Mo_3(\mu\text{-}O)_2(\mu\text{-}S)(\mu_3\text{-}CCPh)[Fe_2(CO)_6(\mu_3\text{-}S)_2]_2$. The redox chemistry of the oxo-containing Mo and W clusters has been investigated, and the molecular structures of five products have been crystallographically determined [117].

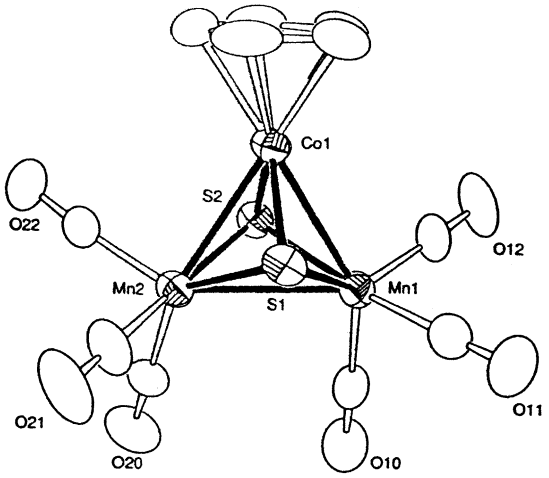

Fig. 10. X-ray structure of $CpCoMn_2(CO)_6(\mu_3\text{-}S)_2$. Reprinted with permission from Organometallics. Copyright 2002 American Chemical Society.

The chiral clusters $(\eta^5\text{-}Cp)(\eta^5\text{-}RCp)(CO)_5MoNiFe(\mu_3\text{-}S)$ (where R = Me, MeCO, MeO_2C) react with $Ru_3(CO)_{12}$ in refluxing toluene to afford the single-tetrahederal clusters $(\eta^5\text{-}RCp)(CO)_8MoRu_2(\mu_3\text{-}S)$ and the double-tetrahedral $Mo_2Ru_2S_2$ co-edged clusters $[(\eta^5\text{-}RCp)(CO)_4MoRu(\mu_3\text{-}S)]_2$. Solution IR and NMR data are reported, and the X-ray structures of three clusters are presented [118]. Thermolysis of the chalcogen-bridged clusters $Fe_3(CO)_9(\mu_3\text{-}E)_2$ (where E = Se, Te) with $CpM(CO)_3(CCPh)$ (where M = Mo, W) in the presence of Me_3NO gives the mixed-metal clusters $CpMFe_2(\mu_3\text{-}E)_2(CO)_6(\eta^1\text{-}CCPh)$. The η^1-coordination mode displayed by the acetylide ligand was confirmed by X-ray diffraction analysis for $CpMoFe_2(\mu_3\text{-}Se)_2(CO)_6(\eta^1\text{-}CCPh)$, whose structure is shown in Fig. 11. The two acetylide-substituted clusters

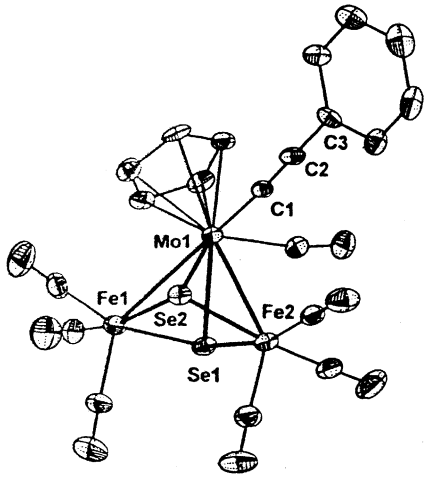

Fig. 11. X-ray structure of $CpMoFe_2(\mu_3\text{-}Se)_2(CO)_6(\eta^1\text{-}CCPh)$. Reprinted with permission from Organometallics. Copyright 2002 American Chemical Society.

(M = Mo, E = Se, Te) react with $Co_2(CO)_8$ to give $CpMoFeCo_2(\mu_3\text{-}E)_2(CO)_9(\mu\text{-}CCPh)$. Schemes accounting for the formation of the observed products are presented and discussed [119].

$Os(CO)_4(CNBu^t)$ reacts with $Mn(CO)_5X$ (where X = Cl, Br) to give $X[Os(CO)_3(CNBu^t)]_nMn(CO)_5$ (where $n = 1, 2, 3$) depending upon the reaction conditions. The Os_2Mn clusters were isolated as two isomers, where the major isomer has an isocyanide ligand attached to each osmium center and the minor isomer has both isocyanide ligands bound to the terminal osmium atom. The molecular structures for these linear-chain isomers have been crystallographically established. The solid-state structures were found to be consistent with the low-temperature ^{13}C NMR data in the carbonyl region of the NMR spectra. A single isomer was found for the Os_3Mn cluster $(OC)_3(I)(^t BuNC)OsOs(CO)_3(^t BuNC)Os(CO)_3(^t BuNC)Mn(CO)_5$, whose composition and linear arrangement of Os-OsOsOsMn atoms were determined by X-ray analysis [120]. New metal clusters have been synthesized by using the carbyne species $[Cp(CO)_2M{\equiv}CPh]^+$ (where M = Mn, Re). The clusters $MRu_2(\mu\text{-}H)(\mu\text{-}CO)_2(\mu_3\text{-}CPh)(CO)_6Cp$ have been obtained from the reaction of the appropriate carbyne reagent and $[Ru_3(CO)_{11}]^{2-}$. The osmium cluster $[Os_3(CO)_{11}]^{2-}$ only reacts with $[Cp(CO)_2Mn{\equiv}CPh]^+$ to produce $MnOs_2(\mu\text{-}H)(\mu\text{-}CO)_2(\mu_3\text{-}CPh)(CO)_6Cp$ and dimeric $[Mn(CO)_2Cp(\mu\text{-}CPh)]_2$. The anionic cluster $[Fe_4(CO)_{13}]^{2-}$ reacts with both carbyne compounds to yield $MFe_2(\mu\text{-}H)(\mu\text{-}CO)_2(\mu_3\text{-}CPh)(CO)_6Cp$. Five structures are presented and a discussion concerning their important structural features is included in this report [121]. The reaction of $Co(CNS)_2$ and $Fe_2(CO)_6S_2$ in the presence of PPh_3 and $LiBEt_3H$ furnishes the mononuclear complex $Co(CO)_3(PPh_3)_2BEt_3$ and $[Fe_2Co(CO)_8(\mu_3\text{-}S)(PPh_3)]^-$. X-ray diffraction analysis of the Fe_2Co cluster confirms the presence of the expected tetrahedral Fe_2CoS core and the coordination of the PPh_3 ligand to the cobalt center. The

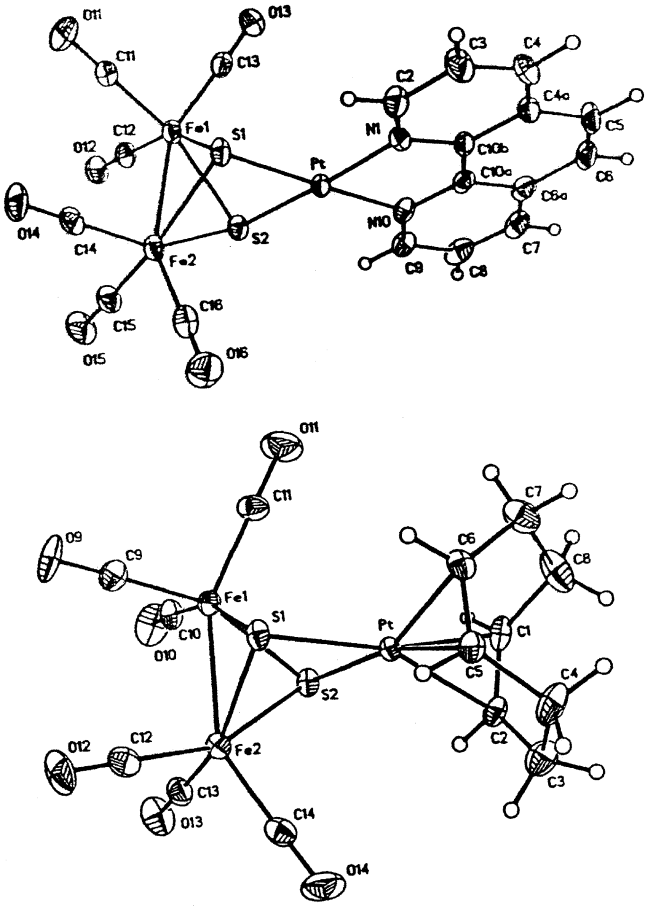

Fig. 12. X-ray structures of $Fe_2(CO)_6(\mu_3\text{-}S)_2Pt(cod)$ and $Fe_2(CO)_6(\mu_3\text{-}S)_2Pt(1,10\text{-phen})$. Reprinted with permission from Organometallics. Copyright 2002 American Chemical Society.

frequency dependent first hyperpolarizability component of this cluster has been determined by using DFT methodology. The MO data indicate that this cluster might function as a second-harmonic generation material of use in optical communication devices [122]. The synthesis and redox properties of the *arachno* clusters $Fe_2(CO)_6(\mu_3\text{-}S)_2PtL_2$ (where L_2 = cod, dppe, bpy, 1,10-phen, dppf) have been reported. Reduction of $Fe_2(CO)_6(\mu_2\text{-}S)_2$ with $LiBEt_3H$, followed by treatment with Cl_2PtL_2, gives high yields of the mixed-metal clusters. The solid-state structures of the cod and 1,10-phen derivatives (Fig. 12) have been determined, with each cluster exhibiting a five-vertex Fe_2S_2Pt core and an unsaturated 16-electron platinum center. The results from extended Hückel MO calculations are presented. The spectroelectrochemical IR and EPR data on the radical anions indicate that the LUMO occurs primarily on the π^* system of the coordinated diimine ligands and on the Fe_2S_2 residue in the case of the diene- and phosphine-substituted derivatives. Excellent agreement was observed between the solution spectroscopic data on the radical anions and the MO calculations [123].

Phosphine replacement in $(CpCo)_2Fe(CO)_2(PPh_3)(\mu_3\text{-}S)(\mu_3\text{-}CS)$ by PR_3 (where R = OMe, OPh, Bu^n) occurs upon heating to afford the corresponding phosphine-

substituted clusters $(CpCo)_2Fe(CO)_2(PR_3)(\mu_3\text{-}S)(\mu_3\text{-}CS)$. Analogous reactions employing isonitriles proceed similarly. The C–S stretching vibration for each capping ligand has been unequivocally identified in each product. NMR measurements indicate that these clusters do not undergo bridge-terminal ligand exchange on the NMR time scale and that the formation of isomers as a result of μ_3-CS and μ_3-CNR scrambling is not observed, which reflects the strong preference of the thiocarbonyl ligand to coordinate to the cluster in a bridging fashion [124]. P–H bond cleavage in Co_2Fe clusters leads to phosphido- and thiophosphido-bridged tetrahedrane clusters. Treatment of $Co_2Fe(\mu_3\text{-}S)(CO)_9$ with Ph_2PH furnishes $Co_2Fe(\mu_3\text{-}S)(CO)_{9-n}(Ph_2PH)_n$ (where $n = 1, 2, 3$). Thermolysis of the mono- and diphosphine-substituted clusters gives $Co_2Fe(\mu_3\text{-}S)(CO)_6(\mu\text{-}PPh_2)_2$ and $Co_2Fe(\mu_3\text{-}S)(CO)_5(\mu\text{-}PPh_2)_2(Ph_2PH)$. The X-ray structure of $Co_2Fe(\mu_3\text{-}S)(CO)_5(\mu\text{-}PPh_2)_2(Ph_2PH)$ indicates that the Ph_2PH is bound to the cobalt center via an equatorial site. Carbonylation of $Co_2Fe(\mu_3\text{-}S)(CO)_6(\mu\text{-}PPh_2)_2$ promotes the coupling of one phosphido group with the capping sulfur group to produce the thiophosphido-capped cluster $Co_2Fe(\mu_3\text{-}SPPh_2)(CO)_7(\mu\text{-}PPh_2)$. The X-ray structures of two additional compounds accompany this report [125]. *cyclo*-$(PhAs)_6$ reacts with $Co_2Fe(\mu_3\text{-}S)(CO)_9$ in toluene at 70 °C to give $Co_2Fe(\mu_3\text{-}S)[\mu\text{-}cyclo\text{-}(PhAs)_6](CO)_7$ as the sole isolated product. The related ligand *cyclo*-$(PhP)_6$ reacts with $Co_2Fe(\mu_3\text{-}S)(CO)_9$ under analogous conditions to afford an isomeric mixture of $Co_2Fe(\mu_3\text{-}S)[\mu\text{-}cyclo\text{-}(PhP)_6](CO)_7$. X-ray analyses reveal that these clusters are isostructural, with the ancillary P and As ligands bridging the cobalt–cobalt bond and exhibiting intact six-membered rings that adopt a chair conformation. Thermolysis reactions of these products leads to cleavage of the ancillary phosphine ligand and formation of $Co_2Fe(\mu_3\text{-}S)(\mu\text{-}\eta^2\text{:}\eta^2\text{:}\eta^1\text{-}P_5Ph_5)(CO)_5$ and complete decomposition of the arsine-substituted cluster. The molecular structures of two thermolysis products are presented [126]. The clusters $Co_2Ni(CO)_6(\mu_3\text{-}\eta^8\text{-}C_8H_6R_2)$ (where R = H, $SiMe_3$) have been isolated from the reaction of $CpNiCo_3(CO)_9$ with cot or 1,4-$(Me_3Si)_2C_8H_6$. Each product was characterized in solution and by X-ray crystallography. These clusters represent the first examples of facially coordinated cot ligands at a heterometallic Co_2Ni triangle [127].

New MnRePt cluster compounds that may be viewed as dithiadimetallic analogues of cymantrene have been synthesized from the reaction of $[MnRe(CO)_6(\mu\text{-}S_2CPR_3)]^{2-}$ with $Pt(cod)Cl_2$. The X-ray structure of $Mn(CO)_3[Pt(cod)(\mu_3\text{-}S)(\mu\text{-}SCPEt_3)Re(CO)_3]$ reveals the existence of a planar, five-membered ring that is composed of the Pt, Re, S, and SC atoms and that is capped by the $Mn(CO)_3$ moiety [128]. The tridentate ligand 2,6-bis(diphenylphosphino)pyridine has been employed in the synthesis of the linear heteronuclear compounds $[Me_2Pt(\mu\text{-}P,N,P\text{-}L_3)_2Ag_2(MeCN)_2]^{2+}$ and $[(CO)_3Fe(\mu\text{-}P,N,P\text{-}L_3)_2Ag_2(Et_2O)]^{2+}$. These two clusters contain a Pt→Ag and Fe→Ag dative bond, respectively, and are stabilized by a d^{10}–d^{10} argentophilic interaction. The electronic absorption data and the emission behavior of these compounds are reported [129]. The reaction of $Pt[Fe(CO)_3(NO)]_2(PhCN)_2$ with diphenyl(2-pyridinyl)phosphine selenide furnishes the 46-electron cluster $(CO)_3Fe(\mu_3\text{-}Se)[Pt(CO)P(2\text{-}C_5H_4N)Ph_2]_2$, whose X-ray structure consists of an open Pt–Fe–Pt triangle that is capped by a μ_3-Se ligand. The bonding in this open cluster has been examined by using DFT and qualitative MO calculations. The bonding is discussed with respect to coordination of two d^{10}-ML_2 fragments to an $(CO)_3Fe{\equiv}S$ unit [130]. The bonding ability of $Co(CO)_3L$ fragments (where L = CO, PPh_3) as building blocks in the construction of PtCo clusters is documented. $[Co(CO)_4]^-$ has been allowed to react with $Pt_2Cl(\mu\text{-}PPh_2)(PPh_3)_3$ (1:1 ratio) to give $Pt_2Co(\mu\text{-}PPh_2)(CO)_4(PPh_3)_2$. X-ray analysis indicates that the two formally monoanionic fragments $[PPh_2]^-$ and $[Co(CO)_4]^-$ bridge a d^9–d^9 Pt(I)–Pt(I) bond. The results of extended Hückel MO calculations are discussed with respect to the possible coordination geometries adopted by the cobalt fragment in this and related compounds [131]. The synthesis of the trinuclear compounds $[Pt_2Ag\{CH_2C_6H_4P(o\text{-}tolyl)_2\text{-}C,P\}_2(\mu\text{-}L)_2]^+$ (where L = pyrazole, 3,5-Me_2pyrazole, 4-Mepyrazole) from $Pt_2\{CH_2C_6H_4P(o\text{-}tolyl)_2\text{-}C,P\}_2(\mu\text{-}L)_2$ and $AgClO_4$ is reported. The Pt_2Ag compounds are shown to contain two Pt–Ag bonds. Reaction of the Pd_2 complex possessing ancillary 3,5-Me_2pyrazole ligands with $AgClO_4$ furnishes $[Pd_2\{CH_2C_6H_4P(o\text{-}tolyl)_2\text{-}C,P\}_2(\mu_3\text{-}3,5\text{-}Me_2pyrazole\text{-}N,N',C^4)_2Ag(\eta^2\text{-}\mu_2\text{-}ClO_4)]$, whose X-ray structure reveals two unprecedented 3,5-Me_2pyrazolate ligands that are bound to the silver center through the C-4 atom of each heterocyclic ring in an η^1 fashion [132]. The reactivity of various phosphido-bridged diplatinum compounds towards electrophiles has been explored. $Pt_2(\mu\text{-}PPh_2)(\mu\text{-}o\text{-}C_6H_4PPh_2)(PPh_3)_2$ reacts with H^+ and $[M(PPh_3)]^+$ (where M = Cu, Ag, Au) at the Pt–Pt bond. The X-ray structure of $[Pt_2\{\mu\text{-}Cu(PPh_3)\}(\mu\text{-}PPh_2)(\mu\text{-}o\text{-}C_6H_4PPh_2)(PPh_3)_2]^+$ consists of a Pt_2Cu triangle that exhibits a bonding interaction between the Cu center and the C_{ipso} of the orthometalated phenyl group. The solution spectral data indicate that the neutral compound $Pt_2[\mu\text{-}AgOC(O)CF_3](\mu\text{-}PPh_2)(\mu\text{-}o\text{-}C_6H_4PPh_2)(PPh_3)_2$ contains a silver atom that is coordinated by a terminally bound $CF_3CO_2^-$ [133].

3.2. Tetranuclear clusters

Thermolysis of $Cp_2Mo_2(\mu\text{-}dmad)(CO)_4$ with excess $Co_2(CO)_8$ gives the expected Mo_2Co_2 cluster $Cp_2Mo_2Co_2(\mu\text{-}dmad)(\mu\text{-}CO)_4(CO)_4$, along with the alkyne-cleaved clusters $Cp_2Mo_2Co_2(\mu_4\text{-}CCO_2Me)_2(\mu\text{-}CO)_2(CO)_8$ and $Cp_2Mo_2Co_5(\mu_4\text{-}CCO_2Me)(\mu_5\text{-}C)(CO)_{12}$. These last two clusters contain unusual edge-sharing bitetrahedral metal frameworks. When acetylene was used in place of dmad, the related carbyne-capped cluster $Cp_2Mo_2Co_5(\mu_4\text{-}CH)(\mu_5\text{-}C)(CO)_{12}$ was isolated and struc-

turally characterized. Carbonylation of $Cp_2Mo_2Co_5(\mu_4\text{-}CCO_2Me)(\mu_5\text{-}C)(CO)_{12}$ leads to the trinuclear cluster $CpMoCo_2(\mu_3\text{-}CCH_2CO_2Me)(CO)_8$, presumably the result of carbide-alkylidyne coupling [134]. The X-ray structures of $(MeCpMo)_2Ir_2(CO)_{10}$ and $(Me_4CpMo)_2Ir_2(CO)_{10}$ have been determined and published [135]. The molecular structures of $CpMoIr_3(CO)_{11}$ (where Cp = Cp, MeCp, Cp*) have been determined and their structural features discussed [136]. The 60-electron clusters $W_2Ir_2(\mu\text{-P-P})(CO)_8(MeCp)_2$ (where P−P = dppe, dppf) have been synthesized from the corresponding decacarbonyl W_2Ir_2 cluster. Both diphosphine ligands are coordinated to adjacent iridium centers via axial coordination. The redox behavior of these products has been investigated by cyclic voltammetry and constant potential coulometry. The dppe-substituted cluster exhibits two reversible, one-electron oxidation waves and an irreversible, two-electron reduction. The dppf derivative shows analogous electrochemical behavior, with an additional irreversible, one-electron oxidation attributed to the ferrocenyl center. The appearance of a low-energy transition in the $1^+/2^+$ redox couple of each product cluster is confirmed by UV-Vis-NIR spectroelectrochemical studies. The X-ray structures of both diphosphine-substituted clusters are presented, with values for the semibridging carbonyl groups discussed [137]. A comprehensive report on the redox properties and spectroelectrochemical data on several tetrahedral Mo_xIr_n clusters has appeared. The clusters $MeCpMoIr_3(CO)_{11}$, $MeCp_2Mo_2Ir_2(CO)_{10}$, and $MeCpWIr_3(CO)_{11}$, $MeCp_2W_2Ir_2(CO)_{10}$, and $Ir_4(CO)_{12}$ were examined by Raman spectroscopy, and these data represent the first Raman spectral studies involving mixed-metal clusters. The molecular structures of $Cp^*MoIr_3(CO)_{11}$, $Cp^*_2Mo_2Ir_2(CO)_{10}$, and $MeCpWIr_3(\mu\text{-}CO)_3(CO)_7(PMe_3)$ (Fig. 13) have been solved and are discussed relative to other structurally characterized clusters of this genre. Synthetic schemes leading to these tetrahedral clusters and the results of DFT calculations are presented and discussed [138].

The reaction of the anionic cluster $[Re_3(\mu\text{-}H)_4(CO)_9(PPh_3)]^-$ with the metallic Lewis acids $[M(PPh_3)]^+$ (where M = Cu, Ag, Au) gives the tetranuclear complexes $Re_3[\mu\text{-}M(PPh_3)](\mu_3\text{-}H)(\mu\text{-}H)_3(CO)_9(PPh_3)$. X-ray structural studies reveal a butterfly Re_3M metal skeleton, where one hydride serves to bridge the Re_2M face and the remaining hydrides span the Re-Re edges. The dissociation of the $[M(PPh_3)]^+$ cations from the Re_3M clusters is controlled by the donor power of the solvent, with dissociation of the silver adduct being rapid on the NMR time scale in acetone solvent. The exchange of the anionic Re_3 cluster with the silver and copper adducts has been investigated by VT ^1H NMR and ^1H 2D-EXSY measurements [139].

A crystallographic study on a new structural isomer of $[CoFe_3(CO)_{13}]^-$ has been published. The new structure contains the expected $CoFe_3$ tetrahedral core but with the ancillary CO ligands exhibiting a different arrangement about the cluster polyhedron relative to the other crystallographically characterized structural isomer. The relationship between the two $CoFe_3$ isomers is discussed with respect to Johnson's Ligand Polyhedral Model [140]. $Ru_3(CO)_{12}$ has been allowed to react with *cis*-Pt(dppe)$(CCPh)_2$ to give an isomeric mixture of $PtRu_3(\mu_4\text{-}\eta^1\text{:}\eta^1\text{:}\eta^2\text{:}\eta^4\text{-}PhCCCCPh)(CO)_{10}(dppe)$. Each isomer contains a 1,4-diphenyl-1,3-butadiyne ligand due to acetylide ligand coupling. The products have been characterized by ^{31}P NMR spectroscopy and X-ray crystallography [141]. Excess vinylacetic acid reacts with $Os_3Rh(\mu\text{-}H)_3(CO)_{12}$ in toluene to produce the new clusters $Os_5Rh_2(\mu\text{-}CO)(\eta^6\text{-}C_6H_5Me)(CO)_{16}$ and $Os_3Rh_2(\mu\text{-}CO)_2(\eta^3\text{-}CH_2CHCH_2COO)_2(CO)_7$. Thermolysis of the Os_3Rh cluster in toluene with added vinylacetate affords $Os_3Rh(\mu_3\text{-}CMe)(\eta^6\text{-}C_6H_5Me)(CO)_9$ and $Os_5Rh_2(\mu\text{-}CO)(\eta^6\text{-}C_6H_5Me)(CO)_{16}$, while thermolysis in toluene alone yields $Os_3Rh(\mu\text{-}H)_3(\eta^6\text{-}C_6H_5Me)(CO)_9$. The isomerization of 1-octene to all isomers of octene is catalyzed by $Os_3Rh(\mu\text{-}H)_3(CO)_{12}$, as verified by GC-MS experiments. The X-ray structures of three products accompany this report [142]. The disulfido-bridged complex $Cp^*Ru(\mu_2\text{-}S_2)(\mu_2\text{-}SPr^i)_2RuCp^*$ reacts with $Pd(PPh_3)_4$ (2 equiv) in refluxing toluene to furnish the 60-electron cluster $(Cp^*Ru)_2(\mu_3\text{-}S)_2Pd_2(\mu_2\text{-}SPr^i)(SPr^i)(PPh_3)$, whose molecular structure consists of a distorted-tetrahedral Pd_2Ru_2 core. Substitution of the thiolate ligands is achieved upon treatment with benzyl bromide, giving $(Cp^*Ru)_2(\mu_3\text{-}S)_2Pd_2(\mu_2\text{-}SPr^i)(Br)(PPh_3)$ and $(Cp^*Ru)_2(\mu_3\text{-}S)_2Pd_2(\mu_2\text{-}Br)(Br)(PPh_3)$, depending on the benzyl bromide stoichiometry. The crystallographic details of five X-ray structures are discussed

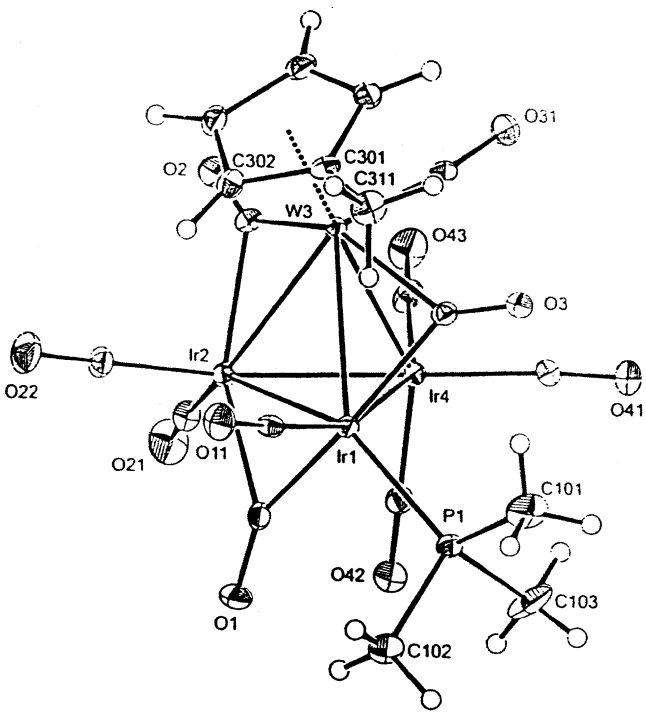

Fig. 13. X-ray structure of $MeCpWIr_3(CO)_7(PMe_3)_4$. Reprinted with permission from Journal of the American Society. Copyright 2002 American Chemical Society.

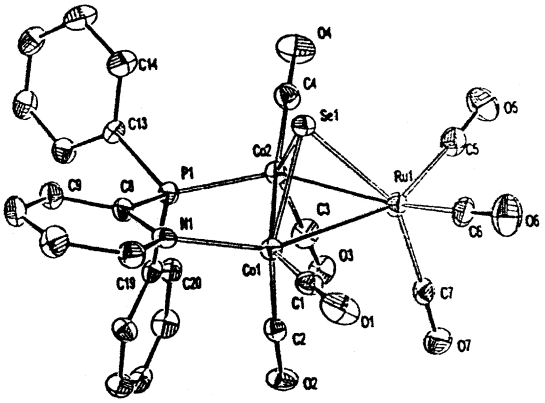

Fig. 14. X-ray structure of $FeCo_2(\mu_3\text{-Se})(CO)_7(\mu\text{-dppy})$. Reprinted with permission from Inorganic Chemistry. Copyright 2002 American Chemical Society.

[143]. Fast and reversible intramolecular cleavage of a Au–C bond in the spiked-triangular clusters $Fe_3Au(\mu_4\text{-}\eta^2\text{-}CCBu^t)(CO)_9(PR_3)$ (where R = Ph, Pr^i) has been demonstrated by NMR measurements and X-ray crystallography [144]. CO exchange in $HMCo_3(CO)_{12}$ and $[MCo_3(CO)_{12}]^-$ (where *M* = *Fe*, Ru) by phosphine selenides such as Ph_3PSe, $Ph_2P(Se)CH_2PPh_2$, $Ph_2(2\text{-}C_5H_4N)PSe$, $Ph_2(2\text{-}C_5H_4S)PSe$, and $Ph[(2\text{-}C_5H_4N)(2\text{-}C_5H_4S)]PSe$ has been explored as a route to selenido-carbonyl bimetallic clusters. The hydrido clusters react with the selenide reagents to give the μ_3-Se capped clusters $MCo_2(\mu_3\text{-Se})(CO)_{9-x}L_y$ (where L = phosphine) and the tetrametal clusters $HMCo_3(CO)_{12-x}L_y$ (where L = deselenized phosphine). The X-ray structures of $FeCo_2(\mu_3\text{-Se})(CO)_7(\mu\text{-dppy})$ (Fig. 14), $RuCo_2(\mu_3\text{-Se})(CO)_7(\mu\text{-dppm})$, and $RuCo_2(\mu_3\text{-Se})(CO)_7(\mu\text{-dppy})$ are reported. These three clusters represent the first structurally characterized mixed-metal clusters containing a capping selenido moiety and an ancillary phosphine ligand. The anionic clusters react only by CO substitution with a deselenized phosphine ligand [145].

Good yields of $Rh_2Pt_2(CO)_6(dppm)$ are reported from the redox condensation of $[Rh(CO)_4]^-$ with $[PtCl(dppm)]_2$ and by the reaction of $Rh_4(CO)_{12}$ with $Pt_2(CO)_3(dppm)_2$. The Rh_2Pt_2 cluster exists as an isomeric mixture in solution. Both isomers have been structurally characterized and found to exhibit a butterfly framework, where the platinum atoms are located at the wingtip positions in these clusters. The isomers differ only by the mode of dppm coordination on the cluster polyhedron. The synthesis of $[Rh_6(\mu_3\text{-}CO)_4(CO)_{10}(\mu_2\text{-}CO)_2][Pt_4(dppm)_3]$ from $Rh_6(CO)_{15}(MeCN)$ and $Pt_2(CO)_3(dppm)_2$ is reported. The X-ray structure of this Rh_6Pt_4 cluster is discussed relative to other structural patterns exhibited by hexa- and tetranuclear cluster frameworks that are linked by dative interactions [146].

3.3. Pentanuclear clusters

The compounds $CpMo(CO)_3(CCPh)$ and $Fe_3(CO)_9(\mu_3\text{-}E)_2$ (where E = S, Se) have been allowed to react under mild heating to produce $(CpMo)_2Fe_3(CO)_8(\mu_3\text{-}E)_2[\mu_5\text{-}CC(Ph)CC(Ph)]$, $(CpMo)_2Fe_4(CO)_9(\mu_3\text{-}E)_2(\mu_4\text{-}CCPh)_2$, and $(CpMo)_2Fe_3(CO)_7(\mu_3\text{-}E)_2[\mu_5\text{-}CC(Ph)C(Ph)C]$. Use of $CpW(CO)_3(CCPh)$ in place of the molybdenum reagent furnishes the cluster products $(CpW)_2Fe_3(CO)_7(\mu_3\text{-}E)_2(\mu_3\text{-}\eta^2\text{-}CCPh)(\mu_3\text{-}\eta^1\text{-}CCH_2Ph)$ and $CpWFe_2(CO)_8(\mu\text{-}CCPh)$. All compounds have been characterized in solution by IR and NMR (^1H, ^{13}C, ^{77}Se) spectroscopies. Seven X-ray structures have been determined and their structural highlights discussed. A plausible reaction scheme illustrating the likely course of events is presented [147]. $Au(PPh_3)Cl$ has been allowed to react with $[Os_4(\mu\text{-}H)_3(CO)_{12}]^-$ to give $Os_4Au(\mu\text{-}H)_3(CO)_{12}(PPh_3)$, whose X-ray structure consists of a distorted Os_4 tetrahedron where one Os-Os edge is bridged by the $Au(PPh_3)$ moiety. The electrochemical behavior of the Os_4Au cluster has been investigated by cyclic voltammetric and coulometric methods. This same cluster catalyzes the oxidative carbonylation of aniline to methyl phenylcarbamate in methanol with good conversion. The higher catalytic activity of the Os_4Au cluster relative to $Os_4(\mu\text{-}H)_4(CO)_{12}$ is attributed to the synergetic effect of the bimetallic cluster [148]. The Ag^+-assisted condensation of $[Mn_2(CO)_8(\mu\text{-}PPh_2)]^-$ with $PdCl_2(P–P)$ leads to formation of $Mn_2Pd_2Ag(\mu\text{-}Cl)(\mu\text{-}PPh_2)_2(\mu\text{-dppm})(CO)_8$ and $MnPd(\mu\text{-}PPh_2)(CO)_4(\eta^2\text{-P-P})$. The Mn_2Pd_2Ag cluster shows a distorted bow-tie structure where the two heterometallic triangles share the common silver center [149]. The synthesis, X-ray structures, and electrochemical properties of $[Cu_3(dppm)_3(\mu_3\text{-}\eta^1\text{-}CCFc)_2]^+$, $[Ag_3(dppm)_3(\mu_3\text{-}\eta^1\text{-}CCFc)_2]^{2+}$, and $Pt_2(dppm)_2(\mu\text{-}\eta^1\text{:}\eta^1\text{-}HC{=}CFc)Cl_2$ have been published. A weak intervalence charge-transfer transition at ca. 1200 nm has been observed in the Cu_3Fe_2 cluster in the presence of $[Cp_2Fe][PF_6]$. The two reversible ferrocene oxidations observed in $[Cu_3(dppm)_3(\mu_3\text{-}\eta^1\text{-}CCFc)_2]^+$ are separated by 110 mV, giving rise to a moderate comproportionation constant (K_c 77). The stability of the oxidized Cu_3Fe_2 cluster is discussed relative to reduced electrostatic repulsions and statistical distributions [150].

3.4. Hexanuclear clusters

Thermolysis of $Fe_2Ru(CO)_9(\mu_3\text{-}E)_2$ (where E = S, Se) with $CpM(CO)_3(CCPh)$ (where M = Mo, W) gives the hexanuclear clusters $Cp_2M_2Fe_2Ru_2(CO)_9(\mu_3\text{-}E)_2(\mu\text{-}CCPh)_2$ and the acetylide-coupled clusters $Cp_2M_2Fe_2Ru(CO)_6(\mu_3\text{-}E)_2[\mu_4\text{-}CC(Ph)C(Ph)C]$. The tail-to-tail coupling of the original acetylide ligands has been crystallographically verified in the case of the Mo_2Fe_2RuS cluster. The X-ray structure of $Cp_2W_2Fe_2Ru_2(CO)_9(\mu_3\text{-}E)_2(\mu\text{-}CCPh)_2$ consists of an $FeRuW_2S$ distorted square pyramid, where a WRu edge is bridged by an $Fe(CO)_3S$ moiety and the RuFe edge is bridged by a $Ru(CO)_3$ unit. The acetylide ligands cap the W_2Ru and FeRuW faces in an $\eta^1\text{:}\eta^1\text{:}\eta^2$ fashion [151]. The synthesis of $PtRu_5(C)(CO)_{15}(PBu^t_3)$ from $Ru_5(C)(CO)_{15}$ and $Pt(PBu^t_3)_2$ at room temperature is described. Depending upon the recrystallization solvent, one

of two isomeric forms of the $PtRu_5$ cluster may be isolated. A structure consisting of a square-pyramidal arrangement of ruthenium atoms and a square base $Pt(PBu^t_3)$ cap has been obtained from hydrocarbon solvents, while a square-pyramidal Ru_5 core that is edge-capped by the $Pt(PBu^t_3)$ moiety has been obtained from diethyl ether as the solvent. VT ^{31}P NMR data suggest that these two isomers are in equilibrium and are interconverted by a reversible breaking and making of two Ru–Pt bonds. Here, the $Pt(PBu^t_3)$ moiety is proposed to rock back and forth between the four-fold Ru_4 site (square-base face) and the twofold edge-bridging Ru_2 site. The ability of the CO groups to stabilize the open coordination geometry is described. The thermodynamic and kinetic parameters associated with this model adatom diffusion process are reported [152]. Treatment of $Ru_3(CO)_{12}$ with $Pd(PBu^t_3)_2$ furnishes the Ru_3Pd_2 cluster $Ru_3(CO)_{12}[Pd(PBu^t_3)]_3$ in moderate yield. The solid-state structure exhibits a central Ru_3 triangle, where each Ru–Ru vector is bridged by a $Pd(PBu^t_3)$ moiety. The Lewis acid behavior of each $Pd(PBu^t_3)$ unit is described. An analogous edge-bridging reaction by $Pd(PBu^t_3)$ moieties in the reaction of $Ru_6(\mu_6\text{-}C)(CO)_{17}$ with $Pd(PBu^t_3)_2$ is presented. Here, an isomeric mixture of the product cluster $Ru_6(\mu_6\text{-}C)(CO)_{17}[Pd(PBu^t_3)]_2$ has been confirmed by spectroscopic and crystallographic methods [153]. The formation of carbide and dicarbide clusters have been obtained from the reaction of $ClCCo_3(CO)_9$ with iron carbonyl anions. When $[Fe_3(CO)_{11}]^{2-}$ is employed as the iron carbonyl reagent in the presence of thallous ions, the 94-electron dicarbide cluster $[Co_5Fe(C_2)(CO)_{17}]^-$ is observed as the major product. The X-ray structure reveals the presence of two distorted Co_3C and Co_2FeC tetrahedra that are linked by a C–C bond and a Co–Co bond (Fig. 15). Similar reactions employing $[Fe_4C(CO)_{12}]^{2-}$ and $[Fe_5C(CO)_{14}]^{2-}$ afford $[Fe_4CoC(CO)_{12}]^{2-}$ and $[Fe_5CoC(CO)_{14}]^{2-}$, respectively. Treatment of $ClCCo_3(CO)_9$ with the ketenylidene-capped cluster $[Fe_3(CO)_9(CCO)]^{2-}$ with added Tl^+ ions gives a species that analyzes as $[\{CCo_3(CO)_9\}C\{Fe_3(CO)_9(CCO)\}]^-$. This unstable cluster undergoes reaction with EtOH, followed by functionalization with $Au(PPh_3)Cl$, to give the cluster $(AuPPh_3)_3Fe_3(CO)_9(CCO_2Et)$. X-ray analysis reveals the existence of a 48-electron Fe_3 equilateral triangle that is face capped by the carbyne ligand and one $AuPPh_3$ moiety. The other two $AuPPh_3$ fragments cap Fe_2Au faces [154].

3.5. Higher nuclearity clusters

The synthesis of the spirocyclic clusters μ_4-$Hg[Os_3(\mu\text{-}PR_2)(\mu\text{-}CO)(CO)_9]_2$ (where R = Ph, Bu^i) is reported from the reaction of $[Os_3(\mu\text{-}PR_2)(CO)_{10}]^-$ and $HgCl_2$ in THF at −90 °C. Each product contains a μ_4-Hg atom that bridges one Os-Os vector in each Os_3 subunit. These two clusters, which were characterized in solution, undergo a rearrangement of the metal skeleton upon heating to produce $(CO)_{10}(\mu\text{-}PR_2)Os_3(\mu_4\text{-}Hg)Os_3(\mu\text{-}PR_2)(\mu\text{-}CO)(CO)_9$. These transformations have been studied by UV-Vis spectroscopy, and the activation parameters have been determined. The latter clusters are highly photosensitive and rearrange upon exposure to sunlight to afford the wheel-shaped cluster compounds $Os_6(\mu_6\text{-}Hg)(\mu\text{-}PR_2)_2(CO)_{20}$. The X-ray structure of the PPh_2 derivative reveals the presence of a mercury atom that is located in the center of an Os_6 ring, as shown in Fig. 16 [155].

Mixed rhodium-nickel carbonyl clusters have been analyzed for their relationship to the 11-vertex deltahedra species In_{11}^{7-} and group 13 polyhedral borane and metalloborane polyhedral geometries. The ability of the Rh/Ni clusters to flatten and compensate for hypoelectronicity is discussed within the context of Wade-Mingos rules [156]. The synthesis and structural characterization of the first high-nuclearity Tl/Pd cluster, $[Tl_2Pd_{12}(CO)_9(PEt_3)_9]^{2+}$, have been reported. This product was isolated in good yield from the reaction of $Pd_{10}(CO)_{12}(PEt_3)_6$ with $Au(PPh_3)Cl$ in the presence of $TlPF_6$. An alternative synthesis of the Tl_2Pd_{12} cluster starting from $Pd_4(CO)_5(PEt_3)_4$ in the

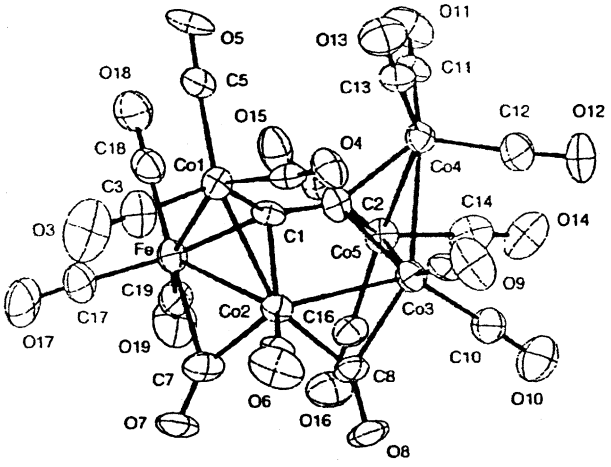

Fig. 15. X-ray structure of $[Co_5Fe(C_2)(CO)_{17}]^-$. Reprinted with permission from Organometallics. Copyright 2002 American Chemical Society.

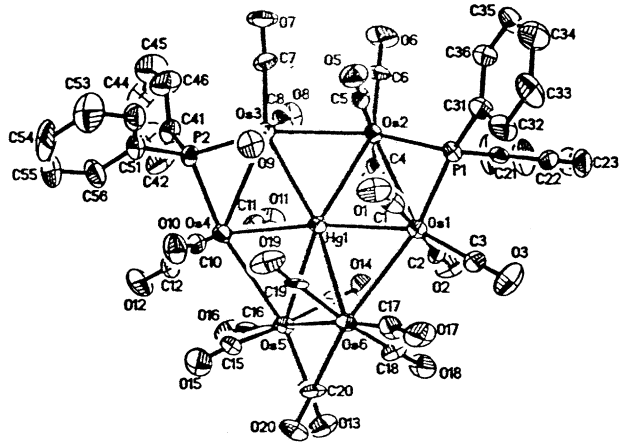

Fig. 16. X-ray structure of $Os_6(\mu_6\text{-}Hg)(\mu\text{-}PPh_2)_2(CO)_{20}$. Reprinted with permission from Organometallics. Copyright 2002 American Chemical Society.

presence of the phosphine scavenger $Au(SMe_2)Cl$ and $TlPF_6$ gives an essentially quantitative yield of the product. The results from gradient-corrected DFT calculations on $Pd_4(CO)_5(PH_3)_4$ are employed in a discussion on the hypothetical Tl^+, Au^+, and $Au(PH_3)^+$ adducts and their relationship to the structure adopted by the Tl_2Pd_{12} cluster [157]. The cluster compounds $[NiRh_{13}(CO)_{25}]^{5-}$, $[Ni_2Rh_{12}(CO)_{25}]^{4-}$, and $[Ni_5Rh_9(CO)_{25}]^{3-}$ have been synthesized from $[RhCl(cod)]_2$ and $[Ni_6(CO)_{12}]^{2-}$. Careful extraction of the product mixture with acetone has led to the isolation of pure $[Ni_5Rh_9(CO)_{25}]^{3-}$, with the separation of the other two anions achieved by subsequent hexane extractions. All three mixed-metal clusters exhibit isostructural cores, and are similar to the homometallic cluster $[Rh_{14}(CO)_{25}]^{4-}$, except for the observed shrinkage of the central Rh_8 cube in the mixed-metal derivatives. The effect of Ni substitution relative to Rh in these clusters has been assessed by extended Hückel MO calculations. The ability to tailor the composition of these clusters is discussed with respect to the MO and redox behavior of this series of isostructural clusters [158]. The synthesis and X-ray structure of the first-known high-nuclearity silver–nickel nanosized cluster, $[Ag_{12}Ni_{24}(CO)_{40}]^{4-}$, have been published. The structural highlights and details from a bonding analysis of this product are discussed [159].

Appendix A

abq	2-amino-7,8-benzoquinoline
bpy	2,2′-bipyridine
cod	1,5-cyclooctadiene
cot	cyclooctatraene
Cp	cyclopentadienyl
Cp*	pentamethylcyclopentadienyl
Cy	cyclohexyl
dmad	dimethyl acetylenedicarboxylate
dppa	1,2-bis(diphenylphosphino)acetylene
dppb	1,4-bis(diphenylphosphino)butane
dppe	1,2-bis(diphenylphosphino)ethane
dppf	1,1′-bis(diphenylphosphino)ferrocene
dppm	bis(diphenylphosphino)methane
dppp	1,3-bis(diphenylphosphino)propane
Fc	ferrocenyl
MAS	magic angle spinning
MeCp	methylcyclopentadienyl
nbd	norbornadiene
PPN	bis(triphenylphosphine)iminium
py	pyridine
tol	tolyl

References

[1] D.E. Insko, Diss. Abstr. Sect. B 63 (2002) 257 (DA3039205).
[2] I.Y. Guzman-Jimenez, Diss. Abstr. Sect. B 63 (2002) 1355 (DA3047312).
[3] K.M. Brosius, Diss. Abstr. Sect. B 63 (2002) 2378 (DA3052016).
[4] D. Dönnecke, Diss. Abstr. Sect. B 62 (2002) 4535 (DANQ62510).
[5] H. Song, Diss. Abstr. Sect. B 63 (2002) 2384 (DA3052131).
[6] G.A. Holloway, Diss. Abstr. Sect. B 62 (2002) 3618 (DA3023076).
[7] C.W. Hills, Diss. Abstr. Sect. B 62 (2002) 3617 (DA3023073).
[8] J.R. Harper, A.J. Lupinetti, A.L. Rheingold, J. Cluster Sci. 13 (2002) 621.
[9] L.Y. Goh, Z. Weng, W.K. Leong, J.J. Vittal, I. Haiduc, Organometallics 21 (2002) 5287.
[10] C. Schulzke, D. Enright, H. Sugiyama, G. LeBlanc, S. Gambarotta, G.P.A. Yap, L.K. Thompson, D.R. Wilson, R. Duchateau, Organometallics 21 (2002) 3810.
[11] L. Xu, K.H. Whitmire, Organometallics 21 (2002) 2581.
[12] L.Y. Goh, Z. Weng, W.K. Leong, P.H. Leung, Organometallics 21 (2002) 4398.
[13] R.D. Adams, O.-S. Kwon, M.D. Smith, Inorg. Chem. 41 (2002) 5525.
[14] R.D. Adams, O.-S. Kwon, M.D. Smith, Inorg. Chem. 41 (2002) 6281.
[15] W.J. Mace, L. Main, B.K. Nicholson, M. Hagyard, J. Organomet. Chem. 664 (2002) 288.
[16] B.F.G. Johnson, S. Tay, Inorg. Chim. Acta 332 (2002) 201.
[17] P.J. King, E. Sappa, C. Sciacca, Inorg. Chim. Acta 334 (2002) 131.
[18] F.W. Vergeer, F. Hartl, P. Matousek, D.J. Stufkens, M. Towrie, Chem. Commun. (2002) 1220.
[19] S. Ko, Y. Na, S. Chang, J. Am. Chem. Soc. 124 (2002) 750.
[20] T. Kondo, Y. Kaneko, Y. Taguchi, A. Nakamura, T. Okada, M. Shiotsuki, Y. Ura, K. Wada, T. Mitsudo, J. Am. Chem. Soc. 124 (2002) 6824.
[21] K. Itami, K. Mitsudo, J. Yoshida, Angew. Chem. Int. Ed. 41 (2002) 3481.
[22] M. Periasamy, C. Rameshkumar, A. Mukkanti, J. Organomet. Chem. 649 (2002) 209.
[23] R. Gobetto, L. Milone, F. Reineri, L. Salassa, A. Viale, E. Rosenberg, Organometallics 21 (2002) 1919.
[24] D. Lentz, S. Willemsen, J. Organomet. Chem. 641 (2002) 215.
[25] G. Süss-Fink, M. Faure, T.R. Ward, Angew. Chem. Int. Ed. 41 (2002) 99.
[26] M. Soleilhavoup, C. Saccavini, C. Lepetit, G. Lavigne, L. Maurette, B. Donnadieu, R. Chauvin, Organometallics 21 (2002) 871.
[27] S.P. Tunik, I.A. Balova, M.E. Borovitiv, E. Nordlander, M. Haukka, T.A. Pakkannen, J. Chem. Soc., Dalton Trans. (2002) 827.
[28] S.-H. Liu, W.S. Ng, H.S. Chu, T.B. Wen, H. Xia, Z.Y. Zhou, C.P. Lau, G. Jia, Angew. Chem. Int. Ed. 41 (2002) 1589.
[29] T. Takao, T. Takemori, M. Moriya, H. Suzuki, Organometallics 21 (2002) 5190.
[30] E. Gatto, G. Gervasio, D. Marabello, E. Sappa, J. Chem. Soc., Dalton Trans. (2002) 1448.
[31] M.I. Bruce, N.N. Zaitseva, B.W. Skelton, A.H. White, J. Chem. Soc., Dalton Trans. (2002) 1678.
[32] F.J. Zuno-Cruz, A.L. Carrasco, M.J. Rosales-Hoz, Polyhedron 21 (2002) 1105.
[33] K. Matsubara, K. Ryu, T. Maki, T. Iura, H. Nagashima, Organometallics 21 (2002) 3023.
[34] M.I. Bruce, B.W. Skelton, A.H. White, N.N. Zaitseva, J. Organomet. Chem. 650 (2002) 188.
[35] R.D. Adams, B. Qu, M.D. Smith, T.A. Albright, Organometallics 21 (2002) 2970.
[36] R.D. Adams, B. Qu, M.D. Smith, Organometallics 21 (2002) 3867.
[37] R.D. Adams, B. Qu, M.D. Smith, Organometallics 21 (2002) 4847.
[38] S. Aime, E. Diana, R. Gobetto, M. Milanesio, E. Valls, D. Viterbo, Organometallics 21 (2002) 50.
[39] H. Song, J.I. Choi, K. Lee, M.-G. Choi, J.T. Parks, Organometallics 21 (2002) 5221.
[40] H. Song, K. Lee, M.-G. Choi, J.T. Park, Organometallics 21 (2002) 1756.

[41] H. Song, C.H. Lee, K. Lee, J.T. Park, Organometallics 21 (2002) 2514.
[42] L.J. Farrugia, P. Mertes, J. Cluster Sci. 13 (2002) 199.
[43] Y.-H. Song, Y. Chi, Y.-L. Chen, C.-S. Liu, W.-L. Ching, A.J. Carty, S.-M. Peng, G.-H. Lee, Organometallics 21 (2002) 4735.
[44] B. Bergmen, E. Rosenberg, R. Gobetto, S. Aime, L. Milone, F. Reineri, Organometallics 21 (2002) 1508.
[45] E. Rosenberg, M.J. Abedin, D. Rokhsana, A. Viale, W. Dastru, R. Gobetto, L. Milone, K. Hardcastle, Inorg. Chim. Acta 334 (2002) 343.
[46] J.A. Cabeza, I. del Río, S. García-Granda, V. Riera, M. Suárez, Organometallics 21 (2002) 5055.
[47] J.A. Cabeza, I. del Río, S. García-Granda, V. Riera, M. Suárez, Organometallics 21 (2002) 2540.
[48] V.A. Ershova, A.V. Golovin, V.M. Porgrebnyak, J. Organomet. Chem. 658 (2002) 147.
[49] S. Aime, F. Bertone, R. Gobetto, L. Milone, A. Russo, M.J. Stchedroff, M. Milanesio, Inorg. Chim. Acta 334 (2002) 448.
[50] V.A. Ershova, A.V. Virovets, V.M. Pogrebnyak, A.V. Golovin, Inorg. Chem. Commun. 5 (2002) 963.
[51] F.W. Vergeer, M.J. Bakker, C.J. Kleverlaan, F. Hartl, D.J. Stufkens, Coord. Chem. Rev. 229 (2002) 107.
[52] F.W. Vergeer, C.J. Kleverlaan, D.J. Stufkens, Inorg. Chim. Acta 327 (2002) 126.
[53] M. Freytag, P.J. Dyson, L. Ernst, P.G. Jones, R. Schmutzler, Inorg. Chem. Commun. 5 (2002) 808.
[54] R.M. DeSilva, M.J. Mays, G.A. Solan, J. Organomet. Chem. 664 (2002) 27.
[55] K. Dallmann, R. Buffon, J. Mol. Catal. A 185 (2002) 187.
[56] A.A. Torabi, A.S. Humphreys, G.A. Koutsantonis, B.W. Skelton, A.H. White, J. Organomet. Chem. 655 (2002) 227.
[57] K.A. Azam, G.M.G. Hossain, S.E. Kabir, K.M.A. Malik, M.A. Mottalib, S. Perven, N.C. Sarker, Polyhedron 21 (2002) 381.
[58] M.I. Bruce, B.W. Skelton, A.H. White, N.N. Zaitseva, J. Cluster Sci. 13 (2002) 235.
[59] P.J. Low, T.M. Hayes, K.A. Udachin, A.E. Goeta, J.A.K. Howard, G.D. Enright, A.J. Carty, J. Chem. Soc., Dalton Trans. (2002) 1455.
[60] E.L. Diz, A. Neels, H. Stoeckli-Evans, G. Süss-Fink, Inorg. Chem. Commun. 5 (2002) 414.
[61] G. Sánchez-Cabrera, F.J. Zuno-Cruz, M.J. Rosales-Hoz, V.I. Bakhmutov, J. Organomet. Chem. 660 (2002) 153.
[62] M. Deng, W.K. Leong, J. Chem. Soc., Dalton Trans. (2002) 1020.
[63] M. Deng, W.K. Leong, Organometallics 21 (2002) 1221.
[64] G. Chen, M. Deng, C.K. Lee, W.K. Leong, Organometallics 21 (2002) 1227.
[65] D. Belletti, D. Cauzzi, C. Graiff, A. Minarelli, R. Pattacini, G. Predieri, A. Tiripicchio, J. Chem. Soc., Dalton Trans. (2002) 3160.
[66] K.A. Azam, K.M. Hanif, A.C. Ghosh, S.E. Kabir, S.R. Karmakar, K.M.A. Malik, S. Parvin, E. Rosenberg, Polyhedron 21 (2002) 885.
[67] S.E. Kabir, K.M.A. Malik, H.S. Mandal, M.A. Mottalib, M.J. Abedin, E. Rosenberg, Organometallics 21 (2002) 2593.
[68] S.N. Konchenko, N.A. Pushkarevsky, M. Scheer, J. Organomet. Chem. 658 (2002) 204.
[69] F.J. Zuno-Cruz, G. Sánchez-Cabrera, M.J. Rosales-Hoz, H. Nöth, J. Organomet. Chem. 649 (2002) 43.
[70] Y. Ohki, N. Uehara, H. Suzuki, Angew. Chem. Int. Ed. 41 (2002) 4085.
[71] M. Martín, E. Sola, F.J. Lahoz, L.A. Oro, Organometallics 21 (2002) 4027.
[72] L.T. Byrne, J.P. Hos, G.A. Koutsantonis, V. Sanford, B.W. Skelton, A.H. White, Organometallics 21 (2002) 3147.
[73] F. Jiang, G.P.A. Yap, R.K. Pomeroy, Organometallics 21 (2002) 773.
[74] L. Scoles, B.T. Sterenberg, K.A. Udachin, A.J. Carty, Chem. Commun. (2002) 320.
[75] L. Scoles, B.T. Sterenberg, K.A. Udachin, A.J. Carty, Can. J. Chem. 80 (2002) 1538.
[76] A.J. Babcock, J. Li, K. Lee, J.R. Shapley, Organometallics 21 (2002) 3940.
[77] R.D. Adams, B. Captain, W. Fu, M.D. Smith, Inorg. Chem. 41 (2002) 2302.
[78] R.D. Adams, B. Captain, W. Fu, M.D. Smith, Inorg. Chem. 41 (2002) 5593.
[79] S.F.A. Kettle, E. Boccaleri, E. Diana, M.C. Iapalucci, R. Rossetti, P.L. Stanghellini, Inorg. Chem. 41 (2002) 3620.
[80] R.D. Adams, B. Captain, W. Fu, M.D. Smith, J. Organomet. Chem. 651 (2002) 124.
[81] M. Faure, H. Stoeckli-Evans, G. Süss-Fink, Inorg. Chem. Commun. 5 (2002) 9.
[82] T. Sugihara, A. Wakabayashi, Y. Nagai, H. Takao, H. Imagawa, M. Nishizaza, Chem. Commun. (2002) 576.
[83] M.C. Comstock, J.R. Shapley, Organometallics 21 (2002) 5983.
[84] F.-E. Hong, S.-C. Chen, Y.-T. Tsai, Y.-C. Chang, J. Organomet. Chem. 655 (2002) 172.
[85] A. Matsubayashi, S. Kuwata, Y. Ishii, M. Hidai, Chem. Lett. (2002) 460.
[86] F. Takagi, H. Seino, Y. Mizobe, M. Hidai, Organometallics 21 (2002) 694.
[87] C. Li, E. Widjaja, W. Chew, M. Garland, Angew. Chem. Int. Ed. 41 (2002) 3786.
[88] Y. Fukumoto, K. Sawada, M. Hagihara, N. Chatani, S. Mutrai, Angew. Chem. Int. Ed. 41 (2002) 2779.
[89] W. Chew, E. Widjaja, M. Garland, Organometallics 21 (2002) 1982.
[90] E. Widjaja, C. Li, M. Garland, Organometallics 21 (2002) 1991.
[91] R. Lazzaroni, R. Settambolo, A. Caiazzo, M.A. Bennett, Organometallics 21 (2002) 2454.
[92] V. Calvo-Perez, A.C. Vega, P. Cortes, E. Spodine, Inorg. Chim. Acta 333 (2002) 15.
[93] M. Costa, G. Gervasio, D. Marabello, E. Sappa, J. Organomet. Chem. 656 (2002) 57.
[94] B.-H. Zhu, W.-Q. Zhang, Q.-Y. Zhao, Z.-G. Bian, B. Hu, Y.-H. Zhang, Y.-Q. Yin, J. Sun, J. Organomet. Chem. 650 (2002) 181.
[95] J. Fiedler, C. Nervi, D. Osella, M.J. Calhorda, S.S.M.C. Godinho, R. Merkel, H. Wadepohl, J. Chem. Soc., Dalton Trans. (2002) 3705.
[96] C. Evans, G.J. Harfoot, J.S. McIndoe, C.J. McAdam, K.M. Mackay, B.K. Nicholson, B.H. Robinson, M.L. Van Tiel, J. Chem. Soc., Dalton Trans. (2002) 4678.
[97] C.M. Ziglio, M.D. Vargas, D. Braga, F. Grepioni, J.F. Nixon, J. Organomet. Chem. 656 (2002) 188.
[98] E. Gullo, S. Detti, G. Laurenczy, R. Roulet, J. Chem. Soc., Dalton Trans. (2002) 4577.
[99] C. Babij, C.S. Browning, D.H. Farrar, I.O. Koshevoy, I.S. Podkorvtov, A.J. Poë, S.P. Tunik, J. Am. Chem. Soc. 124 (2002) 8922.
[100] R.D. Pergola, A. Bianchi, F.F. de Biani, L. Garlaschelli, M. Manassero, M. Sansoni, D. Strumolo, P. Zanello, Organometallics 21 (2002) 5642.
[101] R.B. King, Inorg. Chim. Acta 334 (2002) 34.
[102] A. Pietrzykowski, P. Buchalski, S. Pasynkiewicz, J. Lipkowski, J. Organomet. Chem. 663 (2002) 249.
[103] J.S.L. Yeo, J.J. Vittal, W. Henderson, T.S.A. Hor, Inorg. Chem. 41 (2002) 1194.
[104] R. Ros, A. Tassan, R. Roulet, G. Laurenczy, V. Duprez, K. Schenk, J. Chem. Soc., Dalton Trans. (2002) 3565.
[105] F. Lemaître, D. Brevet, D. Lucas, A. Vallat, Y. Mugnier, P.D. Harvey, Inorg. Chem. 41 (2002) 2368.
[106] R. Stadnichenko, B.T. Sterenberg, A.M. Bradford, M.C. Jennings, R.J. Puddephatt, J. Chem. Soc., Dalton Trans. (2002) 1212.
[107] L.R. Falvello, J. Forniés, C. Fortuño, F. Durán, A. Martín, Organometallics 21 (2002) 2226.
[108] P. Leoni, F. Marchetti, M. Pasquali, L. Marchetti, A. Albinati, Organometallics 21 (2002) 2176.
[109] C. Femoni, M.C. Iapalucci, G. Longoni, P.H. Svensson, Inorg. Chim. Acta 330 (2002) 111.

[110] Y.-Y. Lin, S.-W. Lai, C.-M. Che, K.-K. Cheung, Z.-Y. Zhou, Organometallics 21 (2002) 2275.
[111] L.-C. Song, W.-F. Zhu, Q.-M. Hu, Organometallics 21 (2002) 5066.
[112] W.-F. Liaw, C.-H. Hsieh, S.-M. Peng, G.-H. Lee, Inorg. Chim. Acta 332 (2002) 153.
[113] R.D. Adams, O.-S. Kwon, M.D. Smith, Inorg. Chem. 41 (2002) 1658.
[114] R.D. Adams, O.-S. Kwon, M.D. Smith, Organometallics 21 (2002) 1960.
[115] M. Brandl, H. Brunner, J. Wachter, M. Zabel, Organometallics 21 (2002) 3069.
[116] M.J. Mays, P.R. Raithby, K. Sarveswaran, G.A. Solan, J. Chem. Soc., Dalton Trans. (2002) 1671.
[117] P. Mathur, S. Mukhopadhyay, G.K. Lahiri, S. Chakraborty, C. Thöne, Organometallics 21 (2002) 5209.
[118] L.-C. Song, G.-H. Zeng, Q.-M. Hu, H.-W. Cheng, H.-T. Fan, J. Organomet. Chem. 656 (2002) 228.
[119] P. Mathur, A.K. Bhunia, A. Kumar, S. Chatterjee, S.M. Mobin, Organometallics 21 (2002) 2215.
[120] F. Jiang, H.A. Jenkins, D.F. Green, G.P.A. Yap, R.K. Pomeroy, Can. J. Chem. 80 (2002) 281.
[121] N. Xiao, Q. Xu, S. Tsubota, J. Sun, J. Chen, Organometallics 21 (2002) 2764.
[122] B. Zhuang, H. Sun, L. He, Z. Zhou, C. Lin, K. Wu, Z. Huang, J. Organomet. Chem. 655 (2002) 233.
[123] A. Morneau, W.E. Geiger, M.G. Richmond, M.-J. Don, W.H. Watson, A. Nagl, Organometallics 21 (2002) 1247.
[124] A.R. Manning, A.J. Palmer, J. Organomet. Chem. 651 (2002) 60.
[125] J.D. King, M.J. Mays, C.-Y. Mo, G.A. Solan, G. Conole, M. McPartlin, J. Organomet. Chem. 642 (2002) 227.
[126] R.M. De Silva, M.J. Mays, P.R. Raithby, G.A. Solan, J. Organomet. Chem. 642 (2002) 237.
[127] H. Wadepohl, S. Gebert, R. Merkel, H. Pritzkow, J. Organomet. Chem. 641 (2002) 142.
[128] D. Miguel, D. Morales, V. Riera, S. García-Granda, Angew. Chem. Int. Ed. 41 (2002) 3034.
[129] H.-B. Song, Z.-Z. Zhang, Z. Hui, C.-M. Che, T.C.W. Mak, Inorg. Chem. 41 (2002) 3146.
[130] C. Graiff, A. Ienco, C. Massera, C. Mealli, G. Predieri, A. Tiripicchio, F. Ugozzoli, Inorg. Chim. Acta 330 (2002) 95.
[131] R. Bender, P. Braunstein, S.-E. Bouaoud, D. Rouag, P.D. Harvey, S. Golhen, L. Ouahab, Inorg. Chem. 41 (2002) 1739.
[132] L.R. Falvello, J. Forniés, A. Martín, V. Sicilia, P. Villarroya, Organometallics 21 (2002) 4604.
[133] C. Archambault, R. Bender, P. Braunstein, Y. Dusausoy, J. Chem. Soc., Dalton Trans. (2002) 4084.
[134] H. Adams, L.V.Y. Guio, M.J. Morris, S.E. Spey, J. Chem. Soc., Dalton Trans. (2002) 2907.
[135] N.T. Lucas, M.G. Humphrey, Acta Crystallogr. C 58 (2002) 171.
[136] N.T. Lucas, I.R. Whittall, M.G. Humphrey, Acta Crystallogr. C 58 (2002) 249.
[137] J.P. Blitz, N.T. Lucas, M.G. Humphrey, J. Organomet. Chem. 650 (2002) 133.
[138] N.T. Lucas, J.P. Blitz, S. Petrie, R. Stranger, M.G. Humphrey, G.A. Heath, V. Otieno-Alego, J. Am. Chem. Soc. 124 (2002) 5139.
[139] T. Beringhelli, G. D'Alfonso, M.G. Garavaglia, M. Panigati, P. Mercandelli, A. Sironi, Organometallics 21 (2002) 2705.
[140] C. Evans, B.K. Nicholson, J. Organomet. Chem. 645 (2002) 281.
[141] S. Yamazaki, Z. Taira, T. Yonemura, A.J. Deeming, A. Nakao, Chem. Lett. (2002) 1174.
[142] J.P.-K. Lau, W.-T. Wong, J. Organomet. Chem. 659 (2002) 151.
[143] S. Kuwata, K. Hashizume, Y. Mizobe, M. Hidai, Organometallics 21 (2002) 5401.
[144] E. Delgado, B. Donnadieu, M.E. García, S. García, M.A. Ruiz, F. Zamora, Organometallics 21 (2002) 780.
[145] P. Braunstein, C. Graiff, C. Massera, G. Predieri, J. Rosé, A. Tiripicchio, Inorg. Chem. 41 (2002) 1372.
[146] I.O. Koshevoy, S.P. Tunik, S. Jääskeläinen, M. Haukka, T.A. Pakkanen, I.S. Podkorytov, J. Chem. Soc., Dalton Trans. (2002) 2768.
[147] P. Mathur, M.O. Ahmed, J.H. Kaldis, M.J. McGlinchey, J. Chem. Soc., Dalton Trans. (2002) 619.
[148] Y. Li, W.-X. Pan, W.-T. Wong, J. Cluster Sci. 13 (2002) 223.
[149] Y. Liu, K.H. Lee, J.J. Vittal, T.S.A. Hor, J. Chem. Soc., Dalton Trans. (2002) 2747.
[150] J.H.K. Yip, J. Wu, K.-Y. Wong, K.-W. Yeung, J.J. Vittal, Organometallics 21 (2002) 1612.
[151] P. Mathur, C. Srinivasu, M.O. Ahmed, V.G. Puranik, S.B. Umbarker, J. Organomet. Chem. 659 (2002) 196.
[152] R.D. Adams, B. Captain, W. Fu, P.J. Pellechia, M.D. Smith, Angew. Chem. Int. Ed. 41 (2002) 1951.
[153] R.D. Adams, B. Captain, W. Fu, M.D. Smith, J. Am. Chem. Soc. 124 (2002) 5628.
[154] R. Reina, O. Riba, O. Rossell, M. Seco, M. Font-Bardia, X. Solans, Organometallics 21 (2002) 5307.
[155] H. Egold, M. Schraa, U. Flörke, J. Partyka, Organometallics 21 (2002) 1925.
[156] R.B. King, Inorg. Chem. 41 (2002) 4722.
[157] S.A. Ivanov, R.V. Nichiporuk, E. Mednikov, L.F. Dahl, J. Chem. Soc., Dalton Trans. (2002) 4116.
[158] D. Collini, C. Femoni, M.C. Iapalucci, G. Longoni, P.H. Svensson, P. Zanello, Angew. Chem. Int. Ed. 41 (2002) 3685.
[159] J. Zhang, L.F. Dahl, J. Chem. Soc., Dalton Trans. (2002) 1269.